Assessment of melt cleanliness in A356.2 aluminium casting alloy using the porous disc filtration apparatus technique

Part I *Inclusion measurements*

L. LIU, F. H. SAMUEL
Département des Sciences Appliquées, Université du Québec à Chicoutimi, Chicoutimi, Québec, Canada G7H 2B1

The present work was undertaken to study the role of the major operating parameters commonly applied in aluminium foundries, as well as the effect of minor alloying elements on inclusion formation in one of the most widely used Al–Si alloys, i.e., A356.2 primary alloy, using the porous disc filtration apparatus (PoDFA) technique. A set of 23 experiments was conducted (each using a melt of 25 kg of fresh alloy material). In each case, four to six successive PoDFA trials were executed. PoDFA samples containing the unfiltered part of the metal (about 5 mm in thickness) in contact with the PoDFA filter were polished for metallographic examination. Inclusion classification and counting were done using the grid method. The present work summarizes the types and concentrations of non-metallic inclusions as well as aluminium oxide films that can occur in this alloy prior to casting.

1. Introduction

Premium-quality castings are an essential requisite for the critical structural components used in aerospace and automotive applications. The production of such castings requires that porosity and inclusions be minimized (or even eliminated) to negate their harmful influence on the mechanical properties so that these properties are then mainly controlled by the microstructure of the casting. Among the more widely used aluminium casting alloys are A356.2 and A357 alloys. These two alloys represent the most popular of heat-treatable Al–Si alloys that are hardened by magnesium silicide precipitation. Alloy A357 is similar to A356, but has a higher magnesium (Mg) content (about 0.5%) and can be heat treated to a higher strength level [1–3]. The alloy also contains a small amount of beryllium (Be) to improve the resistance of the liquid melt to oxidation, as well as to improve the morphology of the iron intermetallics [4].

The detrimental effects of the presence of inclusions in aluminium are well documented. Although much work has been reported on the study of inclusions, the problem of measuring metal cleanliness through a sensitive quantitative method still exists. The difficulty is further compounded by the fact that the inclusions to be measured are usually very small, about 10–20 mm in diameter, and present in trace amounts (about 10 ppm). The main inclusions that occur during melting of aluminium alloy or holding periods prior to casting are aluminium oxide (Al_2O_3) as dispersed particles or oxide films, aluminium carbide (Al_4C_3), magnesium oxide (MgO), spinel ($MgAl_2O_4$), titanium diboride (TiB_2), aluminium boride (AlB) and titanium aluminide ($TiAl_3$) [5–12].

The porous disc filtration apparatus (PoDFA) technique was introduced as a method of assessing metal cleanliness by Alcan [13]. Using this method, the factors controlling the precipitation and sedimentation of non-metallic inclusions (with dimensions between 20 and 50 μm) could be evaluated. In the present work, the melt cleanliness of A356.2 premium quality alloy was assessed, using the PoDFA technique. This alloy was selected for study because of its wide application in automotive and aerospace applications. The main objective is to study the effect of various foundry parameters and minor alloying elements (recycling) on the type and concentration of inclusions and aluminium oxide films that can occur in A356.2 alloy melts prior to casting. In some cases, commercial C357 alloy was used for comparison purposes.

2. Experimental procedure

2.1. Melt preparation

Table I shows the chemical composition of the A356.2 and C357 alloys. The alloy was received in the form of 12.5 kg ingots that were cut into two halves. The cut pieces were cleaned with ether and then dried in an electric oven prior to being transferred into the melting crucible. Melting was done in an electric resistance furnace, using silicon carbide crucibles of 35 kg capacity.

0022–2461

TABLE I Chemical composition of the as-received A356.2 and C357 alloy ingots

Alloy	Amount (wt %) of the following elements						
	Si	Mg	Fe	Mn	Cu	Be	Sr
A356.2	6.78	0.33	0.11	0.04	0.02	—	—
C357	7.06	0.56	0.048	0.007	0.012	0.017	0.0015

Fluidity of the liquid metal as a function either of foundry parameters or of minor alloying elements was measured using a 4210 Ragone fluidity tester, where the length of solidified metal in the tester tube (at 200 Torr metallostatic pressure) indicated the corresponding fluidity. PoDFA trials were carried out following the instructions established by Alcan International Limited, Arvida Research and Development Centre, Jonquière, Québec, Canada. The principle of the PoDFA test is outlined schematically in Fig. 1a, while the pore size distribution of the filter is shown in Fig. 1b.

For each experiment, a charge of 25 kg of as-received alloy (or, in some cases scrap) was melted in a 35 kg capacity crucible. The inner walls of the crucible were coated with a thin layer of refractory material to avoid interaction between the liquid metal and the crucible material. When the melt temperature reached 735 $\pm$ 5 °C, the required melt treatment was given, followed by repeated surface skimming, prior to executing the PoDFA test. In each experiment, four to six successive PoDFA trials were carried out, separated by about 40 min intervals, the time required to complete one trial and to bring the melt temperature back to 735 °C for the next trial. The filtration time was taken as the time needed to filter 1.5 kg of the liquid metal from the PoDFA crucible.

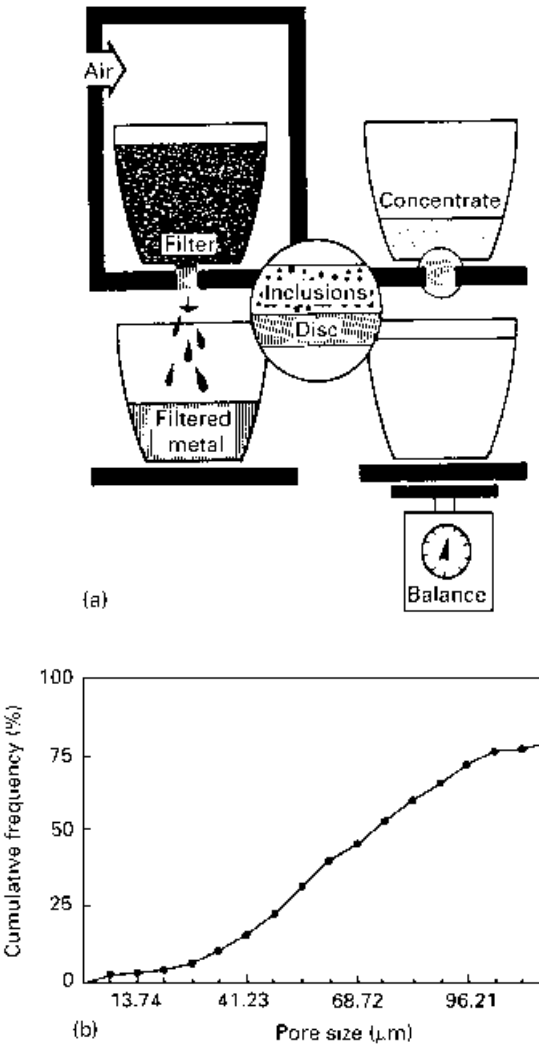

Figure 1 (a) Principle of the PoDFA apparatus, (b) pore size distribution of the PoDFA filter.

2.2. Inclusion measurements

The PoDFA samples (circled in Fig. 1a) containing the unfiltered part of the metal (about 5 mm) in contact with the filter, were hot mounted in Bakelite and polished to a mirror-like finish. Using the grid method, the total inclusion area was obtained. This area was then divided by the mass of the metal that had passed through the filter (about 1.5 kg). The method of inclusion identification is proprietary to Alcan International Limited. The total inclusion concentration area per kilogram was calculated using the formula:

$$\text{total inclusion (mm}^2\text{ kg)} = \frac{\text{mean measured residue area (mm}^2) \times \text{inclusion area fraction}}{\text{filtered metal mass (kg)}} \times \frac{\text{nominal chord length (mm)}}{\text{measured chord length (mm)}}$$

where the inclusions were classified into two categories:

(i) total inclusions that take into account all types of inclusions existing in the 'cake' above the filter, and

(ii) harmful inclusions which are the sum of Al_4C_3 greater than 3 μm, dispersed Al_2O_3, MgO, $MgAl_2O_4$, and potential chlorides (fine Al_4C_3 inclusions of 3 μm or less and TiB_2 have no harmful effect on the alloy mechanical properties).

3. Results and discussion

3.1. Inclusion type and concentration

3.1.1. Foundry parameters

The experimental conditions applied in the present work simulated those used in production foundries and are summarized in Tables II and III. A set of 20 experiments (each using a melt of 25 kg) was carried out to investigate the following variables.

1. *Settling time.* During melting, the molten metal surface was isolated from the surrounding atmosphere

TABLE II Effect of foundry parameters for A356.2 alloy; melt temperature about 735 ± 5 °C (except for experiments 4 and 5 where the melt temperature was about 850 °C, i.e., superheat); PoDFA crucible temperature about 850 °C

Experiment number	Type of charge	Charge (kg)	Settling time (hr)	Stirring speed rev min^{-1}	Stirring time (min)	Degassing time (min)	Filter size (ppi)
1	Fresh	25	0[a]	—	—	—	—
2	Fresh	25	4[a]	—	—	—	—
3	Fresh	25	0[a]	—	—	—	—
4	Fresh	25	0[a]	—	—	—	—
5	Fresh	25	4[a]	—	—	—	—
6	Scrap	25	0[a]	—	—	—	—
7	Scrap	25	4[a]	—	—	—	—
10	Fresh	25	0[b]	125–130	30	—	—
11	Fresh	25	4[b]	125–130	30	—	—
8	Scrap	25	0[b]	125–130	30	—	—
9	Scrap	25	4[b]	125–130	30	—	—
14	Fresh	25	0[b]	125–130	—	45	—
15	Fresh	25	4[b]	125–130	—	45	—
12	Scrap	25	0[b]	125–130	—	45	—
13	Scrap	25	4[b]	125–130	—	45	—
18	Fresh	25	0[a]	—	—	—	10
16	Scrap	25	0[a]	—	—	—	10
17	Scrap	25	0[b]	125–130	—	45	10
19A, 19B	Fresh	25	0[b]	125–130	—	45	10
19C, 19D			0[b]	125–130	—	45	20
19E	Fresh	—	0[b]	125–130	—	45	30
20A, 20B	Fresh	25	72[a]	—	—	—	—
20C, 20D			72[a]	—	—	—	10
20E, 20F			72[a]	125–130	—	45	10

[a] Settling time before stirring and/or degassing.
[b] Settling time after stirring and/or degassing.

TABLE III Effect of foundry parameters for C357 alloy

Experiment number	Type of charge	Charge (kg)	Settling time (hr)	Stirring speed rev min^{-1}	Stirring time (min)	Degassing time (min)	Filter size (ppi)
24A	Fresh	25	0[a]	—	—	—	—
24B			0[a]	—	—	—	10
24C			4[a]	—	—	—	—
24D			4[a]	—	—	—	10
24E			4[a]	—	—	—	20
24F			0[a]	125–130	10	—	—
24G			0[a]	125–130	10	—	10
24H			2[a]	125–130	10	—	10
25A	Fresh	25	72[a]	—	—	—	—
25B				—	—	—	10
25C				125–130	—	45	—
25D				125–130	—	45	10
25E*				—	—	—	—
25F*				—	—	—	10
25G*				—	—	—	20

The asterisks indicate experiments in the cold chamber.
[a] Settling time before stirring and/or degassing.

by covering the top portion of the furnace with a thick plate of refractory material (commercially known as B3). Once the molten temperature reached 735 ± 5 °C, the inclusions were allowed to settle to the bottom of the crucible. The settling time was varied between 0 and 72 h. Prior to executing the PoDFA trial, the dross was carefully skimmed, collected and weighed.

2. *Superheating*. The molten metal temperature was allowed to increase to 850 °C (about 120 °C above the normal working temperature), at which temperature the metal was held for 1 h. Thereafter, it was allowed to cool to 735 °C prior to executing the PoDFA trial.

3. *Type of initial charge*. Two types of initial material were used: fresh ingots and scrap. In both cases, the charge materials were cleaned with ether and dried at 400 °C prior to melting.

4. *Stirring*. Once the molten metal temperature reached the required temperature (735 ± 5 °C), a preheated graphite impeller was introduced into the melting crucible. The rotation speed selected was 120–130 rev min^{-1}, sufficient to agitate the molten

metal but without the introduction of the oxide films formed at the surface of the liquid metal.

5. *Degassing.* In this case, a continuous stream of high-purity argon gas was passed into the molten metal through the graphite impeller. Degassing was done for about 40–50 min, using the same rotation speed of 120–130 rev min^{-1}.

6. *Filtration.* Ceramic foam filter (10, 20 and 30 ppi) discs were placed at the bottom of ceramic pouring cups and fixed in place using refractory cement. The pouring cups were pre-heated to 800 °C and then held above the PoDFA crucible. The molten metal was then poured through these cups and into the PoDFA crucible. It is evident that at such a high temperature, the molten metal would be reoxidized on passing from the pouring cups to the PoDFA crucible (the size of the pouring cup being a fraction of that of the PoDFA crucible). Nevertheless, this method would eventually prevent the coarse oxides and dross from entering into the molten metal.

3.1.2. Minor alloying elements

Tables IV and V show the experimental conditions simulating some of the important foundry daily operations such as modification, grain refining and melt chemistry adjustment. The explanation of the codes used in the present work is given in Table VI, the chemical composition of the liquid metal in the different cases in Table VII, and the concentrations of the various additives in Table VIII for the A356.2 alloy.

1. *Modification.* Strontium (Sr) is the main modifying agent used by most aluminium foundries [14–16]. The maximum allowable level to achieve a complete modified structure in A356.2 alloy is about 300 ppm. In the present work, Sr was added in the form of Al–10 wt% Sr master alloy (about 250–300 ppm Sr).

2. *Grain refining.* TiB_2 is found to be the most effective grain-refining agent [17–19] in the case of aluminium alloys [17–19]. It is normally added in the form of Al–Ti–B master alloy, i.e. as Al–5 wt% Ti–1 wt% B, Al–5 wt% Ti–5 wt% B, Al–2.5 wt% Ti–2.5 wt% B or Al–10 wt% Ti–1 wt% B. In the present work, Al–5 wt% Ti–1 wt% B was used. The concentration of TiB_2 was calculated on the basis of a 0.02 wt% Ti addition (with respect to the weight of the molten metal that was required to be treated). In some cases Al–10 wt% Ti was added as grain refiner.

3. *Magnesium addition.* Mg is normally added to A357 in concentrations ranging between 0.45 and 0.7 wt%. It combines with Si to form the age-hardening compound Mg_2Si. This compound, when precipitated from solid solution during heat treatment, is responsible for the improvement in mechanical strength [1]. The change in mechanical properties resulting from heat treatment is due to the fine coherent precipitation of Mg_2Si.

4. *Beryllium addition.* Be is also added to A357 alloy in small quantities, of the order of 0.05 wt%, to improve the precipitation hardening response of the alloy upon artificial ageing [20]. It is added in the form of Al–5 wt% Be master alloy.

5. *Intermetallics.* Sludge is one of the important intermetallics that may form when the concentrations of Fe, Mn and Cr impurities exceed the allowable limit. Such contamination occurs when steel tools such as skimmers, ladles and stirrers are used without proper coating. Sludge particles are formed in the liquid state. Because of their higher density, they tend to precipitate to the bottom of the melting crucible. The formula used to calculate the possibility of sludge formation or sludge factor (SF) is given by [21]

$$SF = [Fe](\%) + 2[Mn](\%) + 3[Cr]\ (\%)$$

When $SF \geqslant 1.8$, the possibility of sludge formation is very high, especially when the molten metal is held for a sufficiently long time at temperatures close to that required for sludge formation (about 680 °C). In the present case, Fe, Mn and Cr were introduced into the molten metal in the form of Al–25 wt% Fe, Al–25 wt% Mn and Al–20 wt% Cr master alloys. The

TABLE IV Effect of minor additives for A356.2 alloy (25 kg per experiment; fresh ingots)

Experiment number	Additives	Stirring speed (rev min^{-1})	Stirring time (min)	Settling time (hr)	Degassing time (min)	Filter size (ppi)
21A, 21B	Sr	125–130	15	0[b]	—	—
21C				2[b]	—	—
21D				2[b]	—	10
21E	TiB_2	125–130	15	0[b]	—	—
21F, 21G	TiB_2	125–130	15	2[b]	—	10
22A, 22B	Sr	125–130	15	0[b]	—	—
22C				2[b]	—	—
22D				2[b]	—	10
22E	TiB_2	125–130	15	0[b]	—	10
22F				2[b]	—	20
22H				2[b]	15	10
23A, 23B	Fe, Mn, Cr	125–130	15	0[b]	—	—
23C, 23D				2[b]	—	—
23E, 23F	Be	125–130	15	0[b]	—	—
23G, 23H				2[b]	—	—
23I	Sr	125–130	10	0[b]	—	—
23J				0[b]	—	10

[b]Settling time after stirring and/or degassing.

TABLE V Effect of minor additives for A357 alloy (25 kg per experiment; fresh ingots)

Experiment number	Additives	Stirring speed (rev min^{-1})	Stirring time (min)	Settling time (hr)	Degassing time (min)	Filter size (ppi)
26A	Sr	125–130	15	0[b]	—	—
26B					—	10
26C					—	20
26D	TiB_2	125–130	15	0[b]	—	—
26E				0[b]	—	10
26F				0[b]	—	20
26G				0[b]	45	—
26H				0[b]		20
27A	TiB_2	125–130	10	0[b]	—	—
27B				0[b]	—	10
27C				12[b]	—	—
27D				12[b]	—	10
28A	Ti	125–130	15	0[b]	—	—
28B				0[b]	—	10
28C				3[b]	—	—
28D				3[b]	—	10
29A	Fe, Mn, Cr	125–130	15	0	—	—
29B				0	—	20
29C	Be	125–130	15	0	—	—
29D				0	—	20
29E	Sr	125–130	15	0	—	—
29F				0	—	20
29G	Ti	125–130	15	0	—	—
29H				0	—	20
29I	TiB_2	125–130	15	0	—	10

[b]Settling time after stirring and/or degassing.

TABLE VI Explanation of codes used in the present work

Code	Explanation				
A0	A: A356				0: settling time is 0 h
AS0	A: A356	S: Sr			0: settling time is 0 h
AS2	A: A356	S: Sr			2: settling time is 2 h
AST0	A: A356	S: Sr	T: TiB_2		0: settling time is 0 h
AST2	A: A356	S: Sr	T: TiB_2		2: settling time is 2 h
AF0	A: A356	F: Fe, Mn, Cr			0: settling time is 0 h
AF2	A: A356	F: Fe, Mn, Cr			2: settling time is 2 h
AFB0	A: A356	F: Fe, Mn, Cr	B: Be		0: settling time is 0 h
AFB2	A: A356	F: Fe, Mn, Cr	B: Be		2: settling time is 2 h
AFBS0	A: A356	F: Fe, Mn, Cr	B: Be	S: Sr	0: settling time is 0 h

TABLE VII Chemical compositions of A356.2 alloy under different melt treatment conditions

Alloy code	Amount (wt%) of the following elements												
	Si	Fe	Cu	Mn	Mg	Cr	Ni	Zn	B	Sn	Sr	V	Ti
A0	7.05	0.108	0.0122	0.0381	0.36	0.00184	0.00642	0.0324	0.00116	< 0.00100	0.00023	0.0135	0.08
AS0	7.03	0.107	0.0126	0.0374	0.36	0.00182	< 0.00650	0.0339	0.00157	< 0.00100	0.0237	0.0134	0.08
AS2	7.04	0.105	0.0121	0.0379	0.353	0.00184	0.00656	0.0326	0.00115	< 0.00100	0.0162	0.0134	0.106
AST0	7.04	0.106	0.0122	0.0371	0.341	0.00203	< 0.00589	0.0321	0.00348	< 0.00100	0.0254	0.0136	0.105
AST2	6.95	0.113	0.0124	0.0363	0.337	0.00175	< 0.00500	0.0309	0.00351	< 0.00100	0.0236	0.0135	0.0803
AF0	6.84	0.714	0.0134	0.459	0.337	0.122	< 0.00610	0.032	0.00517	< 0.00100	0.00034	0.014	0.0754
AF2	6.68	0.711	0.013	0.455	0.33	0.12	< 0.00500	0.0308	0.00488	< 0.00100	0.00029	0.0137	0.0731
AFB0	6.66	0.706	0.0131	0.44	0.324	0.117	< 0.00500	0.0298	0.00495	< 0.00100	0.00056	0.015	0.0729
AFB2	6.59	0.699	0.0129	0.445	0.337	0.119	< 0.00570	0.03	0.00531	< 0.00100	0.00099	0.0149	0.0734
AFBS0	6.78	0.684	0.0136	0.477	0.33	0.119	< 0.00643	0.0308	0.00466	< 0.00100	0.031	0.0146	0.0736

TABLE VIII Concentrations of additives in A356.2 alloy

Alloy code	Amount (wt%) of the following elements													
	Si	Fe	Cu	Mn	Mg	Cr	Ni	Zn	B	Sn	Sr	V	Ti	
AS0	− 0.02	− 0.001	0.0004	− 0.0007	0	− 0.00002	< 0.00007	0.0015	0.00041	0	0.02347	− 0.0001	0	
AS2	− 0.01	− 0.003	− 0.0001	− 0.0002	− 0.007	0	0.00014	0.0002	− 0.00001	0	0.01597	− 0.0001	0.026	
AST0	− 0.01	− 0.002	0	− 0.001	− 0.019	0.00019	< − 0.00053	− 0.0003	0.00232	0	0.02517	− 0.0001	0.025	
AST2	− 0.1	0.005	0.0002	− 0.0018	− 0.023	− 0.00009	< − 0.00142	− 0.0015	0.00235	0	0.02337	0	0.0003	
AF0	− 0.21	0.606	0.0012	0.4209	− 0.023	0.12016	< − 0.00032	− 0.0004	0.00401	0	0.00011	0.0005	− 0.0046	
AF2	− 0.37	0.603	0.0008	0.4169	− 0.03	0.11816	< − 0.00142	− 0.0016	0.00372	0	0.00006	0.0002	− 0.0069	
AFB0	− 0.39	0.598	0.0009	0.4019	− 0.036	0.11516	< − 0.00142	− 0.0026	0.00379	0	0.00033	0.0015	− 0.0071	
AFB2	− 0.46	0.591	0.0007	0.4069	− 0.023	0.11716	< − 0.00072	− 0.0024	0.00415	0	0.00076	0.0014	− 0.0066	
AFBS0	− 0.27	0.576	0.0014	0.4389	− 0.03	0.11716	< 0.00000999	− 0.0016	0.0035	0	0.03077	0.0011	− 0.0064	

concentrations of these elements were calculated in such a way that SF was higher than 1.8, in order to study the effect of sludge on inclusion formation and precipitation.

In all the above-mentioned cases, the molten metal was mechanically stirred for 10–15 min after the addition of each alloying element to ensure its proper dissolution into the liquid metal.

From the above experiments, the data on

(i) filtration time (for 1.5 kg of filtered metal),
(ii) length of solidified tubes (Ragone fluidity tests),
(iii) total inclusions ($mm^2\ kg^{-1}$),
(iv) total harmful inclusions ($mm^2\ kg^{-1}$),
(v) types and concentrations of inclusions and
(vi) oxide films

was obtained and are summarized in Tables IX–XII for both foundry parameters and minor alloying element additions. The inclusion concentrations have been arbitrarily classified into five classes: class (1), very light; class (2), light; class (3), moderate; class (4), heavy and class (5), excessive. These correspond to the total inclusion concentrations of 0–0.05, 0.05–0.1, 0.1–0.4, 0.4–1.2 and greater than 1.2 $mm^2\ kg^{-1}$, respectively. The casting quality expected to result from such an inclusion concentration can be summarized as excellent (very light and light), acceptable (moderate), acceptable scrap (heavy), and rejected scrap (excessive).

3.2. Examples of inclusions

An example of a graphite inclusion is shown in Fig. 2. It appears as a long thin brown layer. The Al_4C_3 particles precipitate in the form of black needles (Fig. 3a to d). Their contrast changes with exposure to the surrounding humidity. These inclusions may have occurred from stirring and/or degassing of the molten metal using a graphite impeller for a fairly lengthy period of time (about 45 min) at temperatures as high as 735 °C. Another possibility for the formation of these inclusions can arise when the molten aluminium reacts with the inner surface of the silicon carbide crucible at places where the coating on the surface has deteriorated. The reaction may be written as

$$4Al + 3SiC \rightarrow 3Si + Al_4C_3$$

It should be noted that Al_4C_3 particles are already present in the commercially pure aluminium ingot used to produce aluminium alloys. The MgO inclusions were seen either in the form of patches with a regular shape (Fig. 4a) or fairly pale in colour (Fig. 4b). Examples of MgO cuboids are shown in Fig. 4c. Fig. 5 shows a classic example of spinel ($MgAl_2O_4$) particles, very dark (almost black) in colour.

Other inclusions that are considered less harmful are potential chlorides and TiB_2. Fig 6a and b consists of bright- and dark-field images, respectively, of potential chlorides. They appear as small roundish holes. Usually, the contours of a hole are crusted with small inclusions that have been collected by the liquid salt (during production of the aluminium ingots). The SrO particles appear as tiny black particles dotting the eutectic silicon particles, in some cases clustered

TABLE IX Filtering parameters and fluidity[a] of A356.2 alloy

Experiment number	Mass of filtered metal (kg)	Filtration time (min)	Length of solidified metal (cm)	Experiment number	Mass of filtered metal (kg)	Filtration time (min)	Length of solidified metal (cm)
Effect of foundry parameters				Effect of foundry parameters			
1A*	1.366	10	36.5	14A	1.454	6	35.8
1B	1.602	7	37	14B	1.479	8	36.5
1C	0.964	6	38.1	14C	1.366	9	35.8
1D	1.074	7	37	14D	1.456	5	36.9
1E	1.627	7	35.5	14E	1.57	4	36.3
2A*	1.418	6	34.7	15A	1.453	5	32.8
2B	1.544	5	34.3	15B	1.454	5	38.1
2C	1.52	5	34.7	15C	1.457	7	35.9
2D	1.399	3	35.5	15D	1.49	5	36.8
2E	1.524	3	34.8	15E	1.48	4	36.7
3A*	1.258	5	—	16A	1.524	5	37.7
3B	1.209	7	—	16B	1.521	3	36.3
3C	1.381	8	—	16C	0.736	5	38
3D	1.518	3	—	16D	1.469	5	37
3E	1.553	4	—	17A	1.481	6	37.6
4A*	1.05	7	34.4	17B	1.446	5	35.2
4B	1.291	7	34.5	17C	1.455	5	35.9
4C	1.467	4	35.2	17D	1.495	6	37.3
4D	1.325	8	35.3	18A	1.452	6	35.7
4E	1.495	5	33.5	18B	1.468	5	36.3
5A*	1.52	5	34.9	18C	1.65	4	36.9
5B	1.505	9	35.7	18D	1.515	7	36.2
5C	1.466	4	34	19A	1.378	6	34.9
5D	1.536	4	35	19B	1.498	4	35.5
5E	1.457	6	34	19C	1.245	5	36
6A*	1.361	6	35.2	19D	1.268	5	36.4
6B	1.498	4	—	19E	1.179	6	35.8
6C	1.706	7	—	20A	1.503	5	36.3
6D	1.278	9	34.2	20B	1.476	6	35.5
6E	1.52	5	36	20C	1.512	4	36.5
7A*	1.506	5	35.5	20D	1.33	6	37.4
7B	1.557	5	36.8	20E	1.174	10	36.1
7D	1.536	5	35.3	20F	1.278	8	34.8
7E	1.534	5	34.8				
8A*	0.944	7	37	Effect of minor additions			
8B	1.505	5	37	21A	1.435	8	35.3
8C	1.477	6	36.3	21B	1.424	11	38.1
8D	1.448	8	37.5	21C	1.011	10	36.3
9A*	1.287	8	36.6	21D	1.48	10	37.1
9B	1.454	7	38.5	21E	0.39	10	36.9
9C	1.441	5	36.5	21F	0.516	10	36.1
9D	1.473	5	37.8	21G	0.494	12	36.8
10A	1.494	7	36.5	22A	1.279	7	37.5
10B	1.294	6	36.5	22B	1.432	5	37.9
10C	1.143	8	37.6	22C	1.442	5	35.6
10D	1.31	9	38	22D	0.67	5	35
10E	1.535	5	35.8	22E	0.252	10	33.7
11A	1.509	8	37.4	22F	0.254	8	36.1
11B	1.447	10	36.7	22G	0.307	5	38
11C	1.32	8	37.2	22H	0.381	11	36.3
11D	1.488	5	41.2	23A	1.228	6	37
11E	1.452	8	36.9	23B	1.466	6	36.3
12A	1.491	5	36.9	23C	1.515	5	—
12B	1.414	9	36	23D	1.47	6	36.1
12C	1.544	5	36	23E	1.504	4	36.5
12D	1.505	7	35.8	23F	1.471	3	37.2
13A	1.49	6	36.1	23G	1.107	4	36.1
13B	1.494	5	36.8	23H	1.535	4	36.9
13C	1.502	5	36.3	23I	1.462	5	36.3
13D	1.502	6	35.2	23J	1.554	5	36.3

The asterisks indicate experiments in the cold chamber.
[a]As measured by the length of solidified metal in the Ragone Fluidity tester tube.

TABLE X Total and harmful inclusion concentrations in A356.2 alloy

Experiment number	Total inclusions ($mm^2\ kg^{-1}$)	Harmful inclusions ($mm^2\ kg^{-1}$)	Experiment number	Total inclusions ($mm^2\ kg^{-1}$)	Harmful inclusions ($mm^2\ kg^{-1}$)
Effect of foundry parameters			Effect of foundry parameters		
1A	0.041	0.009	12C	0.93	0.483
1B	0.041	0.01	12D	0.37	0.222
1C	0.256	0.049	13A	0.153	0.069
1D	0.088	0.02	13C	0.18	0.097
2A	0.034	0.008	13D	0.286	0.194
2B	0.032	0.007	14A	0.159	0.119
2C	0.023	0.006	14D	0.181	0.145
2E	0.015	0.002	14E	0.021	0.019
3A	0.044	0.008	15A	0.221	0.188
3B	0.041	0.011	15D	0.03	0.023
3C	0.043	0.012	15E	0.173	0.138
3D	0.047	0.015	16A	0.1	0.074
3E	0.079	0.021	16B	0.034	0.028
4A	0.041	0.013	16D	0.131	0.118
4B	0.078	0.032	17A	1.405	1.124
4C	0.084	0.029	17B	0.239	0.187
4D	0.063	0.027	17D	0.362	0.286
4E	0.076	0.034	18A	1.129	0.395
5A	0.062	0.031	18C	1.252	0.363
5B	0.05	0.031	18D	0.636	0.35
5C	0.033	0.018	19B	0.032	0.01
5D	0.048	0.034	19D	0.151	0.017
5E	0.054	0.035	19E	0.87	0.07
6A	0.035	0.016	20A	4.244	3.777
6B	0.026	0.011	20C	2.151	1.979
6C	0.013	0.002	20F	1.285	1.105
6D	0.037	0.009			
6E	0.034	0.009			
7A	0.061	0.049	Effect of minor additions		
7D	0.119	0.08	21B	0.24	0.07
7E	0.078	0.047	21D	0.139	0.026
8B	0.035	0.032	21F	6.437	0.515
8C	0.051	0.027	22B	0.07	0.056
8D	0.227	0.182	22C	0.092	0.077
9B	2.628	2.076	22E	1.679	0.084
9C	0.139	0.115	22F	0.826	0.091
9D	0.129	0.125	22G	0.277	0.033
10A	0.244	0.024	22H	1.122	0.123
10D	0.678	0.244	23B	0.432	0.237
10E	0.543	0.19	23D	1.01	0.687
11A	1.489	0.476	23F	0.824	0.511
11B	1.172	0.445	23H	0.766	0.398
11E	1.113	0.579	23I	1.05	0.892
12A	0.852	0.213	23J	0.902	0.793

together. The presence of these oxide particles may explain the formation of porosity in Sr-modified Al–Si castings [22].

The TiB_2 inclusion particles are normally pushed to the interdendritic cell regions, forming a "cake" that seals the filter pores as shown in Fig. 7a and b. This observation may explain the fact that the addition of a small amount of TiB_2 resulted in increasing the filtration time to 15 min in order to collect only 300 g of filtered metal, compared with 3 min for 1.5 kg of filtered metal obtained without TiB_2 addition.

Fig. 8a illustrates examples of "thin oxide films". They appear as pencil line-like defects, i.e., they show no measurable thickness at the optical level. An example of "thick oxide films" is shown in Fig. 8b. As can be seen, these films have a measurable width compared with the former.

Figs 9–16 indicate the experimental conditions that maximize the concentration of each type of inclusion. Figure 9 shows that graphite mainly occurs when stirring and/or degassing using a graphite impeller is applied. Potential chlorides are found in very small amounts, of the order of $0.0008\ mm^2\ kg^{-1}$ (Fig. 10a). The maximum attainable quantity ($0.0065\ mm^2\ kg^{-1}$) of fine potential chlorides is shown in Fig. 10b, corresponding to the case when the molten metal was vigorously stirred. Coarse potential chlorides can occur in amounts of $\sim 0.26\ mm^2\ kg^{-1}$.

Fig. 11a and b shows the experimental conditions corresponding to maximum concentration of fine Al_4C_3 (3 μm or less) inclusions. It is evident that stirring coupled with long holding periods leads to the formation of this type of inclusion. When degassing is applied, a large part of the fine Al_4C_3 particles is removed (Fig. 11b). Since these inclusions are very small, filtration using 10 ppi ceramic foam filter discs may not be sufficient to hinder their motion and

TABLE XI (a) Concentrations of major inclusions in A356.2 alloy

Experiment number	TiB_2 and TiC ($mm^2\ kg^{-1}$)	Al_4C_3 ($\leq 3\ \mu m$) ($mm^2\ kg^{-1}$)	Al_4C_3 ($> 3\ \mu m$) ($mm^2\ kg^{-1}$)	MgO ($mm^2\ kg^{-1}$)	MgO (cuboids) ($mm^2\ kg^{-1}$)	$MgAl_2O_4$ ($mm^2\ kg^{-1}$)
Effect of foundry parameters						
1A	0.0061	0.0253	0.0094	—	—	—
1B	0.0062	0.0257	0.0095	—	—	—
1C	0.0332	0.1738	0.0486	—	—	—
1D	0.0097	0.058	0.0202	—	—	—
2A	0.004	0.0219	0.0078	—	—	—
2B	0.0032	0.0221	0.0071	—	—	—
2C	0.0022	0.0146	0.0059	—	—	—
2E	0.003	0.0094	0.0018	0.0003	—	0.0001
3A	0.0065	0.0285	0.0065	0.0008	—	0.0008
3B	0.0057	0.0237	0.0081	0.0012	—	0.0016
3C	0.0043	0.0269	0.0094	—	—	0.0021
3D	0.007	0.0243	0.0117	0.0009	—	0.0028
3E	0.0087	0.0491	0.0214	—	—	—
4A	0.0061	0.0216	0.013	—	—	—
4B	0.0094	0.0361	0.0314	0.0008	—	—
4C	0.0109	0.0438	0.0295	—	—	—
4D	0.0094	0.0264	0.0264	0.0006	—	—
4E	0.0076	0.0332	0.034	—	—	—
5A	0.0094	0.0212	0.0312	—	—	—
5B	0.009	0.01	0.0299	—	—	0.001
5C	0.005	0.01	0.0181	—	—	0.0003
5D	0.0058	0.0087	0.0315	—	—	0.0024
5E	0.0082	0.0109	0.0332	—	—	0.0022
6A	0.0052	0.0138	0.0138	—	—	0.0017
6B	0.0015	0.0129	0.0093	—	—	0.0021
6C	0.0013	0.0096	0.002	—	—	0.0003
6D	0.0026	0.0251	0.0033	0.0007	—	0.0049
6E	0.0041	0.021	0.0034	0.0007	—	0.0052
7A	0.0031	0.0092	0.0354	—	—	0.0012
7D	0.0036	0.0356	0.0463	—	—	0.0036
7E	0.0117	0.0195	0.0117	—	—	0.0078
8B	0.0035	—	0.0053	0.0007	0.0238	0.0018
8C	0.0041	0.0205	0.0128	—	0.0128	0.001
8D	0.0114	0.0341	0.1566	0.0068	0.0182	—
9B	0.1577	0.3941	0.2102	0.1314	1.524	0.2102
9C	0.0097	0.0139	0.0208	0.0069	0.0735	0.0139
9D	0.0039	—	0.0233	0.0763	0.0258	—
10A	0.039	0.1802	0.0195	0.0024	—	0.0024
10D	0.0813	0.3524	0.0678	0.0474	0.1017	0.0203
10E	0.0706	0.2824	0.0543	0.0597	0.0434	0.0272
11A	0.1489	0.8634	0.2977	0.1489	0.0149	0.0149
11B	0.1758	0.5508	0.293	0.1406	—	0.0117
11E	0.167	0.3674	0.3897	0.167	0.0111	0.0111
12A	—	0.6393	0.1705	0.0426	—	—
12C	—	0.4462	0.3718	0.0744	0.0093	0.0279
12D	—	0.148	0.1813	0.037	—	0.0037
13A	0.003	0.0812	0.0459	—	0.0183	0.0045
13C	0.0071	0.0755	0.0539	0.0035	0.0359	0.0035
13D	0.0057	0.0858	0.1429	0.0086	0.0143	0.0286
14A	—	0.0398	0.1114	0.0079	—	—
14D	0.009	0.027	0.1264	0.018	—	—
14E	—	0.0016	0.0139	0.0052	—	—
15A	0.011	0.022	0.1699	0.0176	—	—
15D	0.0006	0.006	0.0199	—	—	0.0036
15E	0.0035	0.0311	0.0104	0.0346	—	—
16A	0.005	0.02	0.055	0.009	0.003	0.007
16B	0.0007	0.0051	0.0027	0.0055	0.0034	0.0164
16D	0.0026	0.0065	0.0196	0.017	0.0118	0.0693
17A	—	0.281	0.5338	0.0281	0.1826	0.3793
17B	—	0.0526	0.0909	0.0024	0.0239	0.067
17D	0.0036	0.0724	0.2101	0.0036	0.0254	0.0471
18A	0.1694	0.5646	0.2145	0.0226	0.0452	0.1129
18C	0.1627	0.7259	0.1627	0.0125	0.0751	0.1126
18D	0.0127	0.2734	0.2544	—	0.0254	0.0636
19B	0.0006	0.0205	0.0019	0.0013	0.0003	0.007
19D	0.0015	0.1331	0.0061	0.003	0.0015	0.0061
19E	0.0087	0.7917	0.0174	0.0087	0.0087	0.0348
20A	0.2546	0.2122	2.0796	0.0849	1.2732	0.3395
20C	0.1076	0.0645	1.1832	0.1721	0.5378	0.0861
20F	0.0129	0.1671	0.0643	0.9512	0.0386	0.0514

TABLE XI(b) Concentrations of major inclusions in A356.2 alloy (mm^2/kg):

Experiment number	TiB_2 and TiC ($mm^2\ kg^{-1}$)	Al_4C_3 ($\leq 3\ \mu m$) ($mm^2\ kg^{-1}$)	Al_4C_3 ($> 3\ \mu m$) ($mm^2\ kg^{-1}$)	MgO ($mm^2\ kg^{-1}$)	MgO (cuboids) ($mm^2\ kg^{-1}$)	$MgAl_2O_4$ ($mm^2\ kg^{-1}$)	SrO (mm^2/kg^{-1})
Effect of minor additions							
21B	0.0024	0.1104	0.0096	0.0168	0.0024	0.0192	0.0216
21D	0.0014	0.0806	0.0028	0.0056	0.0014	0.0083	0.0083
21F	5.4069	0.2575	0.1287	0.0644	—	0.0644	0.2575
22B	0.0049	0.0063	0.0035	0.0395	—	0.0021	0.0106
22C	0.0018	0.011	0.0036	0.0679	—	0.0027	0.0027
22E	1.4607	0.1343	0.0167	0.0335	0.0167	—	0.0167
22F	0.6858	0.0495	0.0165	0.0413	—	0.0082	0.0165
22G	0.2269	0.0166	0.0027	0.0083	0.0027	0.0055	0.011
22H	0.9197	0.0672	0.0112	0.0224	—	0.0112	0.0672
23B	0.1252	0.0604	0.1511	0.0561	0.0043	0.0215	—
23D	0.2221	0.0908	0.3736	0.1514	0.0403	0.111	—
23F	0.1401	0.1565	0.2966	0.0659	0.0082	0.1318	—
23H	0.1762	0.1916	0.2912	0.0383	0.0076	0.0536	—
23I	0.0419	0.1154	0.3149	0.4199	0.0209	0.1259	—
23J	0.0541	0.0541	0.2434	0.3967	0.009	0.1352	—

TABLE XII Evaluation of Al_2O_3 oxide films in A356.2 alloy

Experiment number	Thin film			Thick film		
	Slight	Moderate	Heavy	Slight	Moderate	Heavy
Effect of foundry parameters						
1A		×				
1B			×			
1C		×				
1D	×					
2A		×				
2B		×				
2C		×				
2E			×			
3A		×				
3B		×		×		
3C		×				
3D			×			
3E	—	—	—	—	—	—
4A	—	—	—	—	—	—
4B		×				
4C		×		×		
4D	×					
4E	×					
5A				×		
5B			×			
5C			×			
5D			×			
5E		×				
6A		×				
6B		×				
6C			×			
6D		×				
6E		×				
7A			×			×
7E			×			×
8C		×				×
8D			×			×
9B	×				×	
9D			×			×
10A		×			×	
10D		×			×	
10E		×			×	
11A		×			×	
11B		×			×	
11E		×			×	
12A	×			×		
12C		×			×	
12D	×			×		

TABLE XII (Continued.)

Experiment number	Thin film			Thick film		
	Slight	Moderate	Heavy	Slight	Moderate	Heavy
13A		×			×	
13C			×			×
13D		×		×		
14D	×			×		
14E		×			×	
15E	×				×	
16A			×			×
16B			×			×
16D			×			×
17A			×		×	
17B			×		×	
17D		×		×		
18A		×			×	
18C		×			×	
18D		×			×	
19B	×			×		
Effect of minor addition						
22C		×		×		
22E	×					
22G		×		×		
22H	×			×		
23B			×			×
23D			×			×
23F			×			×
23H			×			×
23I			×			×
23J			×			×

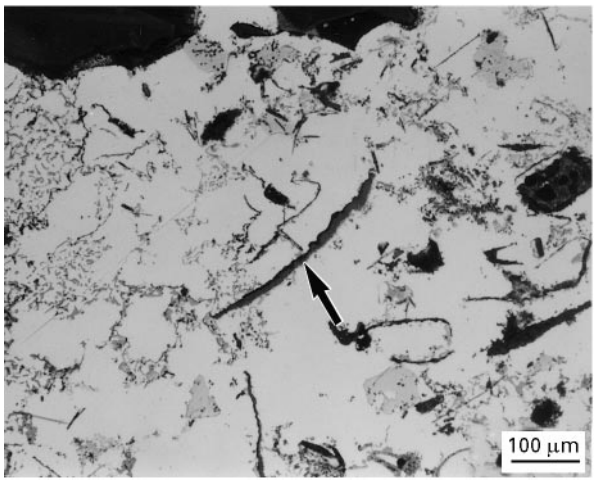

Figure 2 Example of graphite particles.

consequent transfer into the PoDFA crucible. Fig. 11c demonstrates the beneficial effect of degassing and settling time in minimizing the concentration of the fine Al_4C_3 inclusion particles.

It is evident from Fig. 12 that holding the liquid metal for periods as long as 72 h enhances the formation of thick Al_4C_3 inclusion particles (greater than 3 μm). This observation may be interpreted, at least partly, as resulting from the reaction between the molten metal and the wall of the melting crucible. It should be borne in mind that this experiment was the twentieth in the series, without changing the crucible or the coating material. It is interesting to note that filtration with 10 ppi ceramic foam filters resulted in a significant reduction in the concentration of the thick Al_4C_3 inclusion particles. Degassing, however, proved to be the most effective method in removing these inclusions.

MgO is the first oxide to form in the magnesium-oxide-type series. It then transforms into MgO cuboids and later on to spinel, i.e., $MgAl_2O_4$. It is obvious that long holding times, i.e., 72 h, would certainly increase the possibility of its formation. The findings of Doutre *et al.* [13] reveal that MgO and spinel tend to settle to the bottom of the melting crucible with time. Similar observations were made in the present study, as can be seen in Fig. 13a. Increasing the holding time to 4 h led to a noticeable increase in the concentration of MgO (from 0.005 to about 0.15 $mm^2\ kg^{-1}$). Prolonged holding times, i.e., 72 h (Fig. 13b), significantly increased the concentration of MgO to 0.9 $mm^2\ kg^{-1}$, that precipitated to the bottom of the melting crucible. Degassing, however, led to the flotation of MgO to the upper portion of the remaining liquid metal. Fig. 13c shows the effect of the type of initial charge, i.e., scrap, on the concentration of MgO inclusions.

Increasing the Mg content to 0.56 wt%, i.e., C357 alloy, resulted in a marginal increase in the concentration of MgO inclusions when the molten metal was still, even for a period of 72 h (Fig. 14a). In fact, sedimentation or filtration (using 10 and 20 ppi filters)

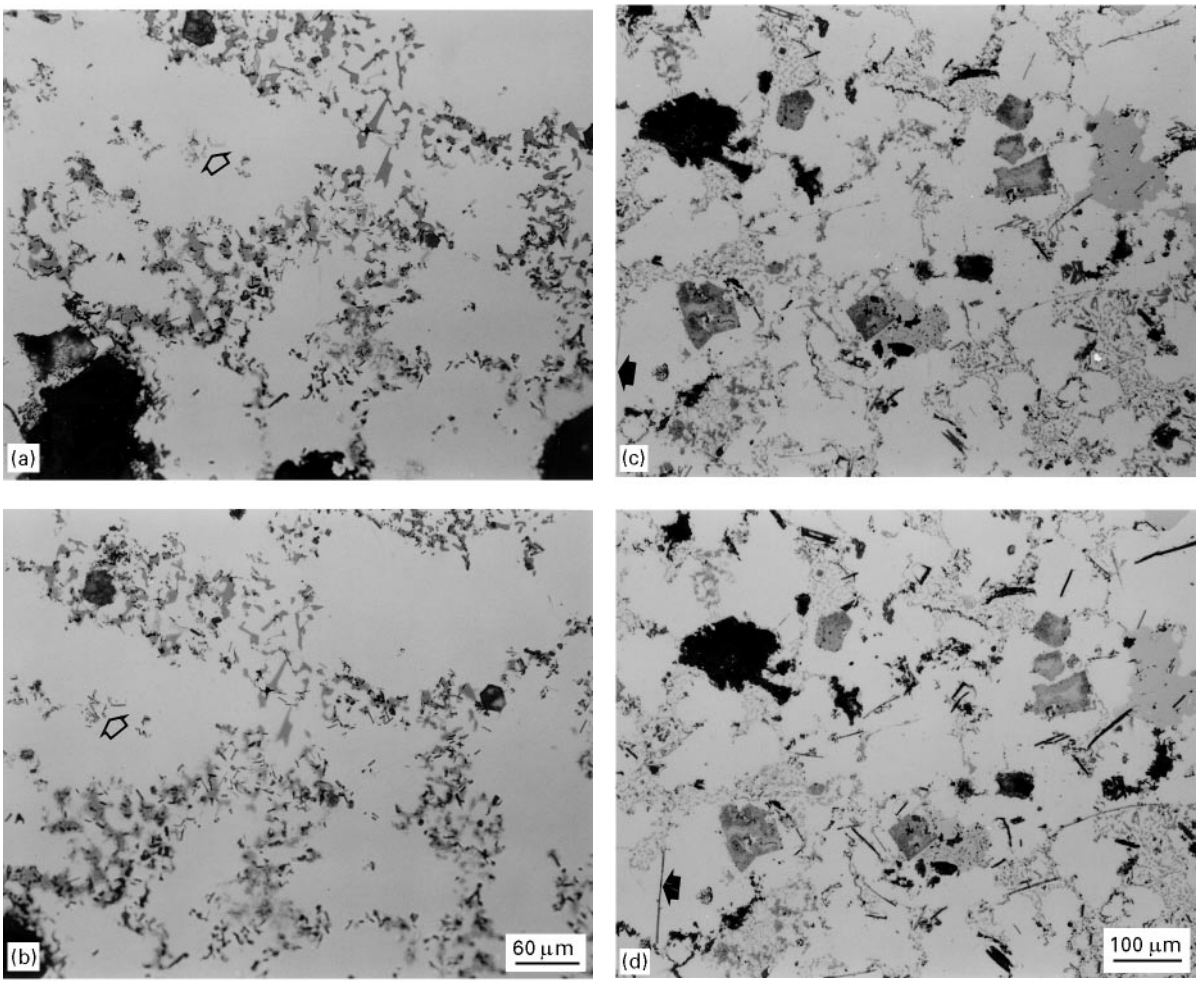

Figure 3 (a), (b) Examples of Al_4C_3 (3 μm or less) particles taken from (a) a freshly prepared sample and (b) after almost a week. (c), (d) Examples of Al_4C_3 (greater than 3 μm) particles taken from (c) a freshly prepared sample and (d) after almost a week.

significantly reduced the MgO concentration as shown in Fig. 14b.

The maximum concentration of the cuboid form of MgO, i.e., 1.4 $mm^2\,kg^{-1}$, was first seen when the scrap was remelted and held for 4 h as shown in Fig. 15a. It is evident that most of the cuboid inclusions have either floated to or formed in the upper portion of the liquid metal, rather than settling to the bottom of the melt crucible. After the first PoDFA trial the concentration of the cuboid inclusions was seen to drop to about 0.07 $mm^2\,kg^{-1}$ for the third PoDFA trial and further to 0.025 $mm^2\,kg^{-1}$ for the fourth PoDFA trial. As expected, holding the liquid metal for 72 h resulted in increasing the concentration of cuboids to 1.3 $mm^2\,kg^{-1}$ in the upper portion of the molten metal, that was relatively more exposed to the surrounding atmosphere. Thus, a gradual reduction in inclusion concentration in the remaining melt is noted in Fig. 15b. Filtration seems effective in removing this type of inclusion.

The cuboid inclusions are found to be much finer in C357 alloy than those reported for A356.2 alloy as exhibited in Fig. 16a, when the molten metal was stagnant. Prolonged holding periods, i.e., 72 h, increased its concentration in the first PoDFA trial, representing the layer that was exposed to the surrounding atmosphere.

Mechanical agitation was more effective in distributing the inclusions that had settled to the bottom of the melting crucible. Allowing the metal to settle increased the concentration of cuboid inclusions in the last PoDFA trials, as displayed in Fig. 16b. In all cases, the concentration of MgO cuboid inclusions was much lower in the C357 alloy than in the A356.2 alloy.

The third inclusion type in the magnesium oxide series, i.e., spinel ($MgAl_2O_4$) was also found to be more concentrated in the upper portion of the molten metal (scrap), together with the MgO cuboids (Fig. 17a). Both types were successfully removed during the first PoDFA trial. Degassing the molten scrap resulted in pushing most of the spinel particles upwards whereas, when the molten metal was kept stagnant, the particles tended to settle near the bottom of the melting crucible (Fig. 17b). Another parameter that significantly contributed to the concentration of spinel inclusions in the upper layer of the molten metal was the increase in holding time, i.e., 72 h, as shown in Fig. 17c. Thus it is recommended that the first and last castings in a series of castings prepared from the same melt be rejected.

The rate of spinel formation was noticeably high in C357 alloy, particularly when the holding time was of the order of 72 h. A large number of the spinel

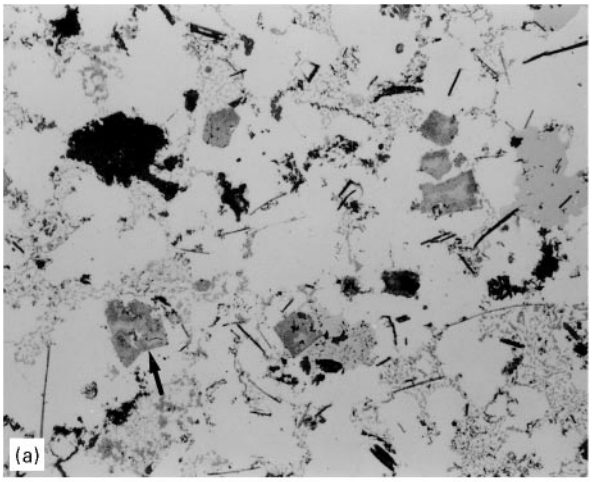

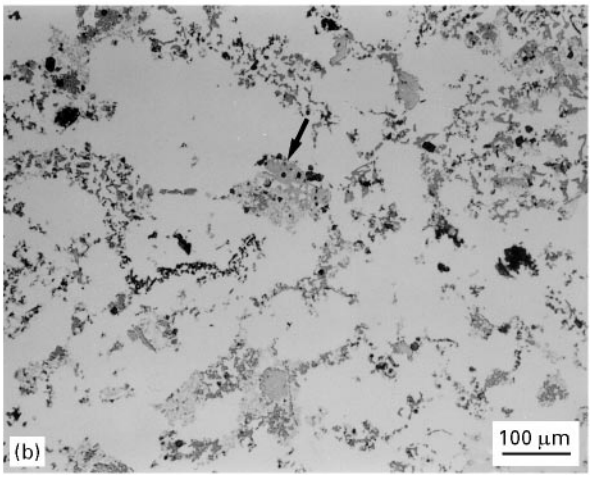

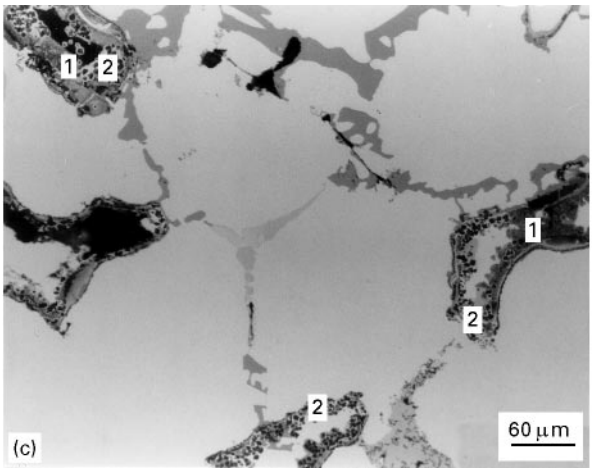

Figure 4 Examples of MgO particles: (a) regular fragments; (b) pale-coloured pieces; (c) MgO (labelled 1) and MgO cuboids (labelled 2) (Note the presence of the two types of magnesium oxide in the same regions).

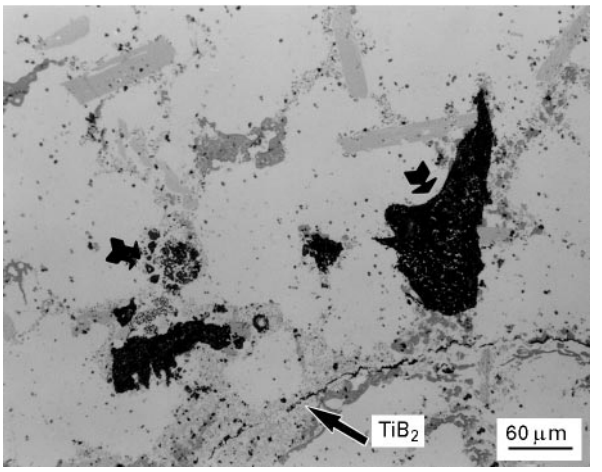

Figure 5 Examples of spinel inclusions. The long platelets are undissolved pieces of Al–Ti–B master alloy.

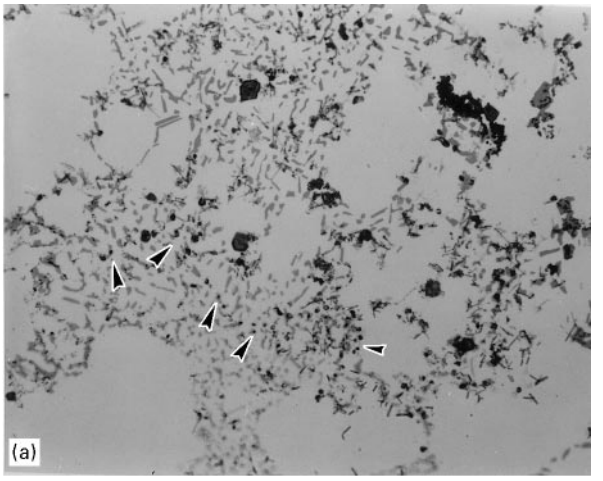

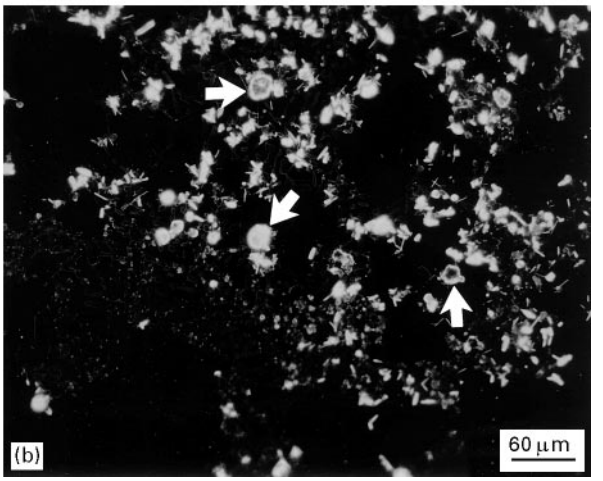

Figure 6 Examples of potential chloride particles: (a) bright-field image; (b) dark-field image (arrows indicate the SrO particles).

inclusion particles was concentrated in the lower portion of the liquid metal as shown in Fig. 18a. Mechanical stirring plus long holding times led to recontamination of the liquid metal, with gradual increase in spinel concentration towards the bottom of the melting crucible (Fig. 18b). The effect of superheat was marginal. Apparently, most of the spinel was formed in the dross that was thoroughly skimmed before executing the PoDFA test.

Fig. 19 shows the experimental conditions that maximize the concentration of the TiB_2 inclusions in Al–Si castings. As shown in Fig. 7, the TiB_2 particles are extremely fine. This observation explains the fact that filtration with 10 ppi ceramic foam filters could not prevent all the TiB_2 particles from entering into the liquid metal. Using finer filters, i.e., 20 ppi, or degassing would be more effective in removing these inclusions. Degassing, however, would lead to

flotation of these particles to the surface of the molten metal. Fig. 20, which shows 10 ppi and 20 ppi ceramic foam filters mounted in pouring cups, clearly demonstrates the difference in their pore sizes.

A comparison of the effects of Sr and TiB_2 addition on the PoDFA filtration behaviour is exhibited in Fig. 21. As can be seen, Sr addition has a marginal or almost no effect on the mass of filtered metal, i.e.,

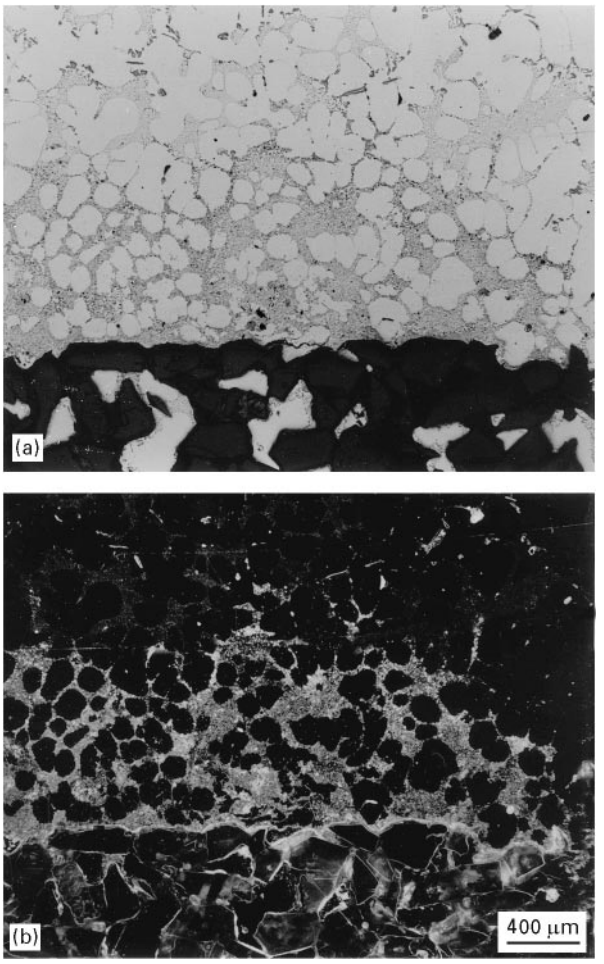

Figure 7 Examples of TiB_2 particles: (a) bright-field image; (b) dark-field image.

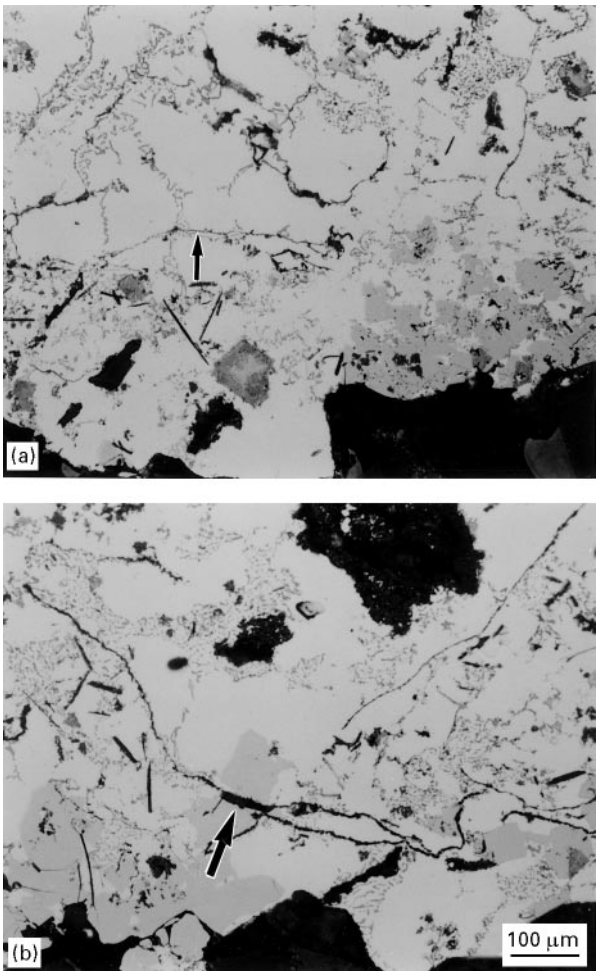

Figure 8 Examples of oxide films: (a) thin film; (b) thick film.

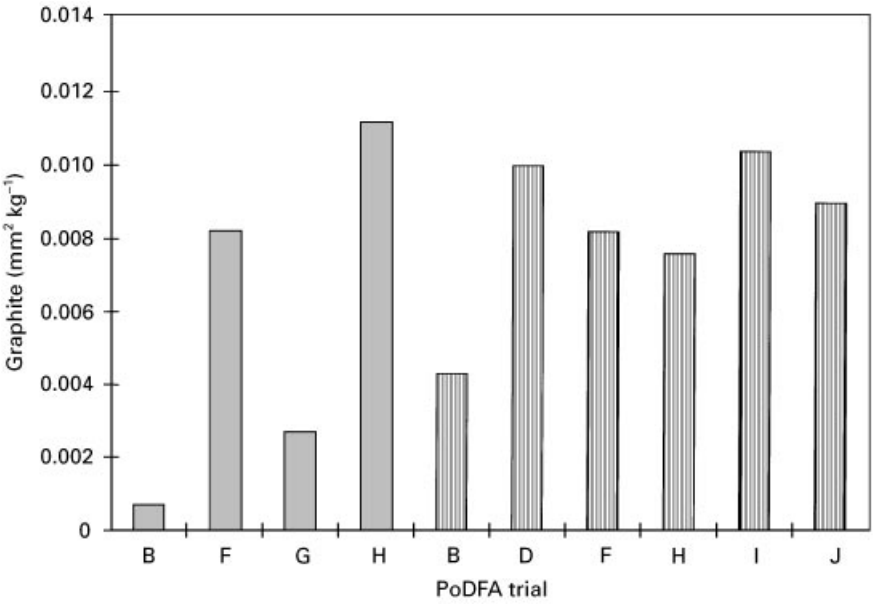

Figure 9 Experimental conditions that maximize the concentration of graphite inclusions. ( ), experiment 22; ( ), experiment 23.

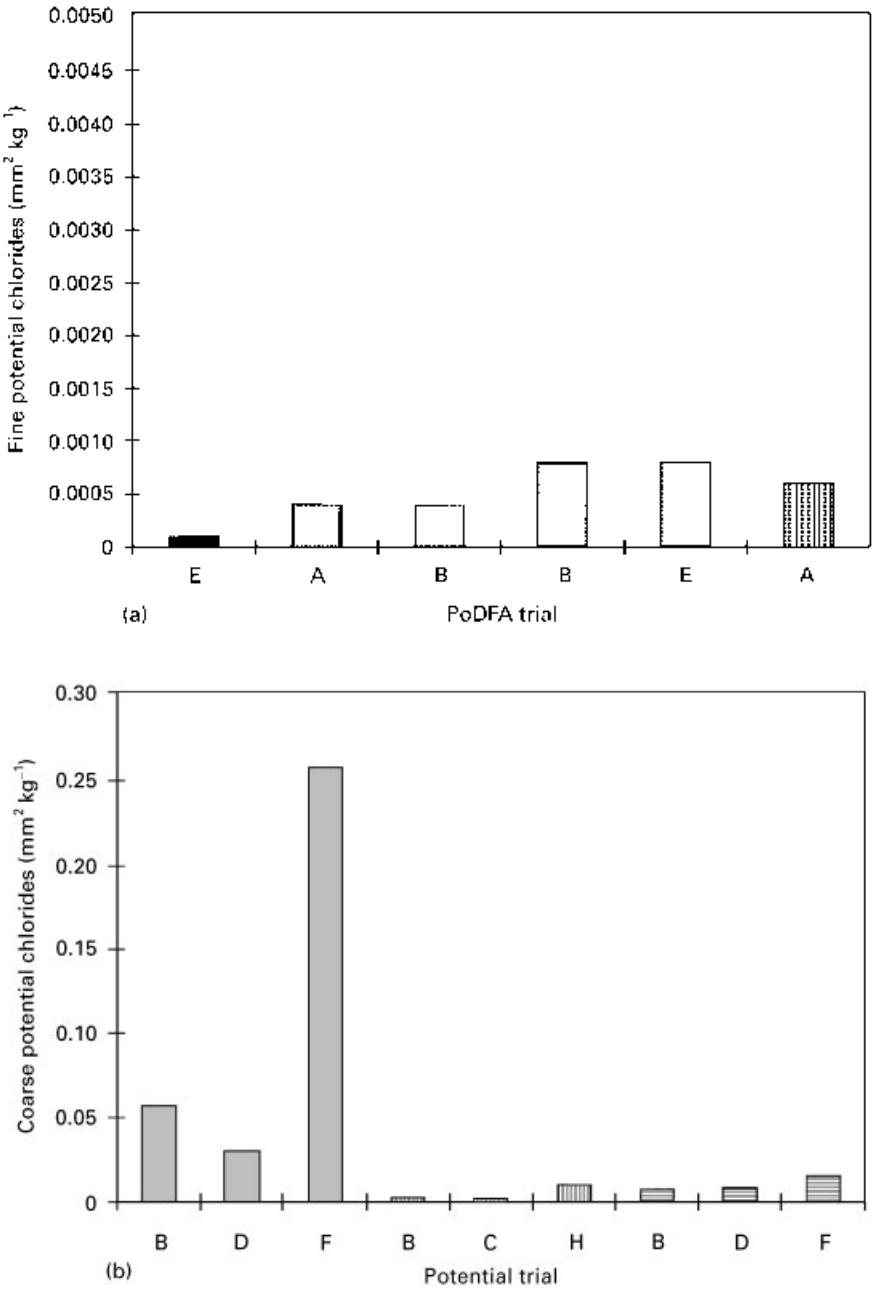

Figure 10 Experimental conditions that maximize the concentration of potential chloride inclusions for (a) fine particles ((▒), experiment 2; (▒), experiment 3; (▒), experiment 4; (▒) experiment 5) and (b) coarse particles.

1.5 kg, compared with that obtained from the unmodified alloy. In contrast, the addition of TiB_2 produces a remarkable reduction in the mass of filtered metal, by almost 80%. This observation is well demonstrated in Fig. 22.

Another interesting parameter to be considered is the lengthy time needed to collect such a small amount (300 g) of filtered metal, as displayed in Fig. 23a. Fig. 23b shows the relationship between the concentrations of SrO and TiB_2 on the filtration time. It is evident that the occurrence of a high density of fine TiB_2 particles would seal the pores of the PoDFA filters (as shown in Fig. 7), leading to the observations documented in Figs 19–22.

Fig. 23c shows the effect of grain-refining agent type, namely, Al_3Ti or TiB_2 on the weight of filtered metal obtained (experiment 29). Evidently, the presence of boron is very effective in increasing the number of TiB_2 particles that act as sites for grain nucleation as examplified in the microstructure in Fig. 24, where the TiB_2 particles are observed abundantly over the entire sample surface.

The main inclusion type that occurs when the alloy is modified with Sr is SrO. The variation in SrO particle concentration depends on the total amount of Sr added to the molten alloy. In the present case, the Sr content, prior to executing the PoDFA trials, was in the range 250–300 ppm. Fig. 25 reveals the tendency of SrO to precipitate towards the bottom of the crucible. When TiB_2 is added to the Sr-modified melt, the SrO particles show a more pronounced tendency to settle down, together with the TiB_2 particles.

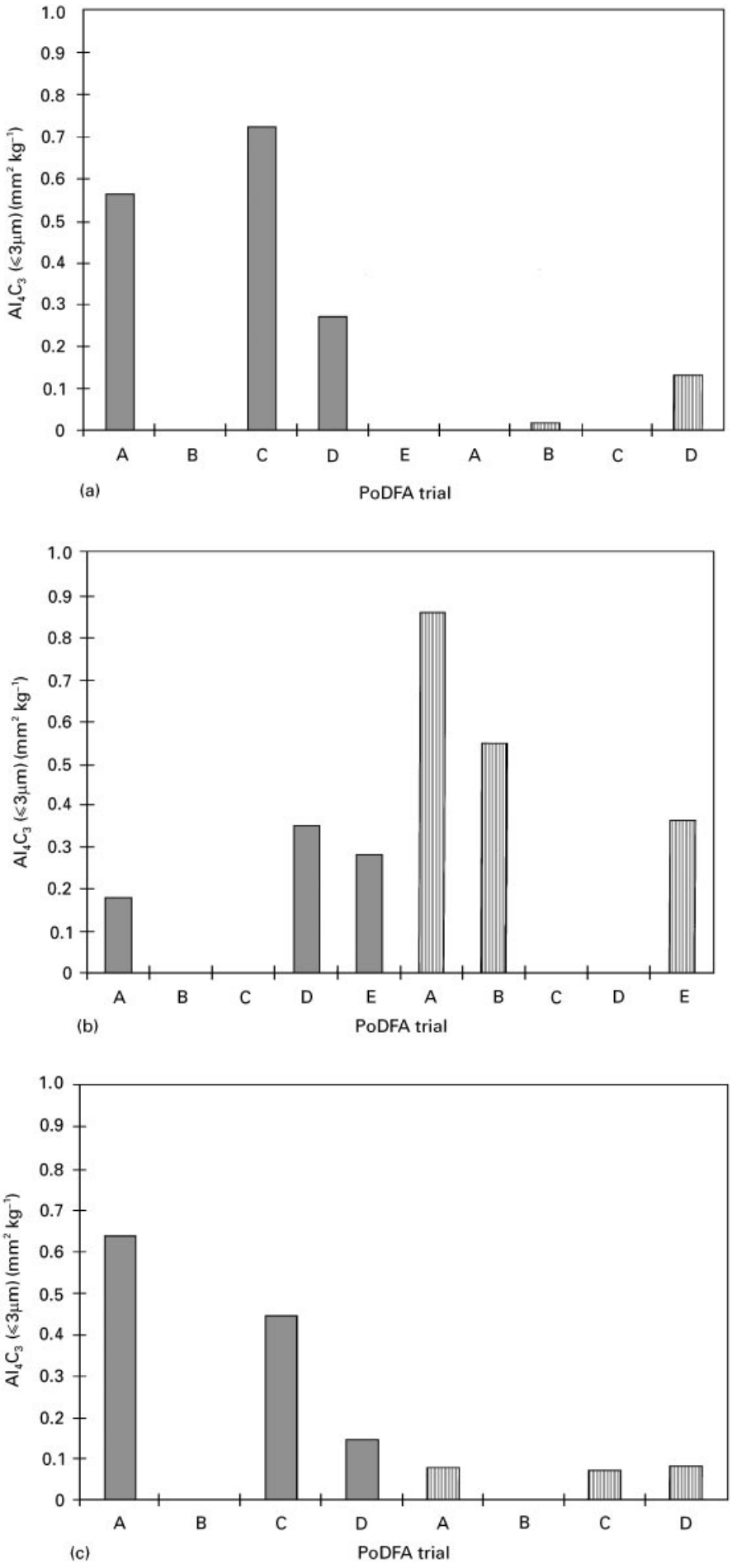

Figure 11 Experimental conditions that maximize the concentration of Al_4C_3 3 μm or less inclusions: (a) effect of mechanical stirring ((▒), experiment 18; (▒) experiment 19); (b) effect of filtration without and with degassing ((▒), experiment 10; (▒), experiment 11) (c) effect of the type of initial charge (▒), experiment 12; (▒), experiment 13).

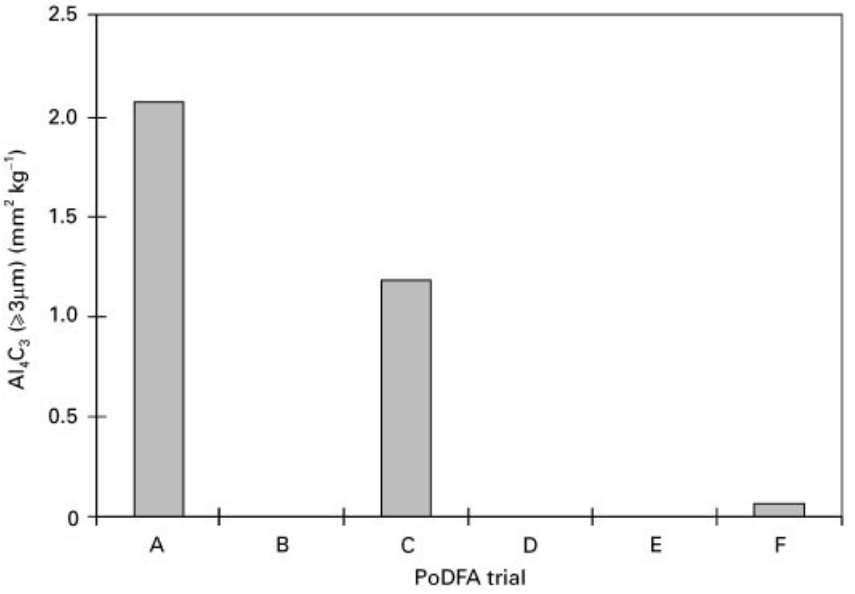

Figure 12 Experimental conditions that maximize the concentration of Al_4C_3 (3 μm or greater) inclusions. ( ), experiment 20.

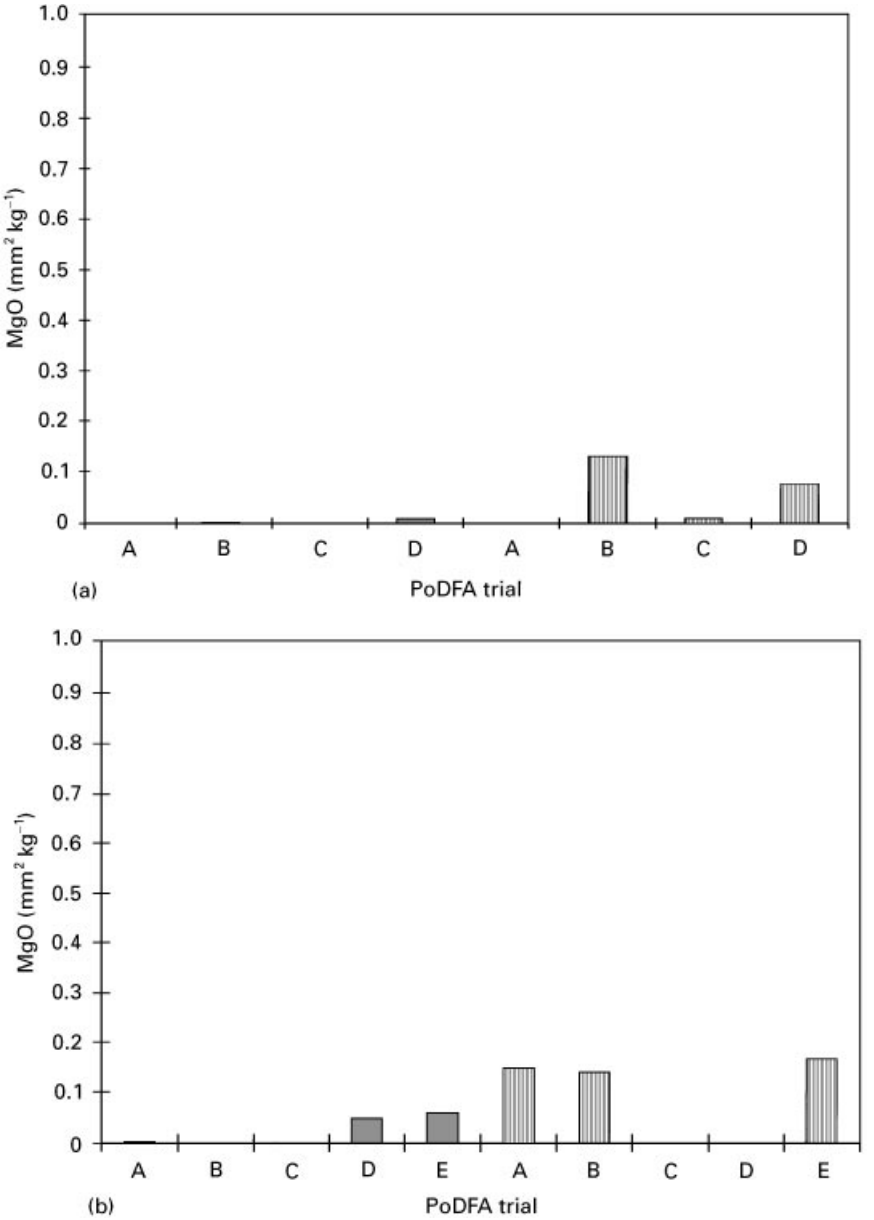

Figure 13 Experimental conditions that maximize the concentration of MgO inclusions in A356.2 alloy: (a) effect of mechanical stirring and settling time (( ), experiment 8, ( ) experiment 9); (b) effect of prolonged holding times, i.e., 72 h (( ); experiment 10; ( ), experiment 11); (c) effect of the type of initial charge (( ), experiment 20).

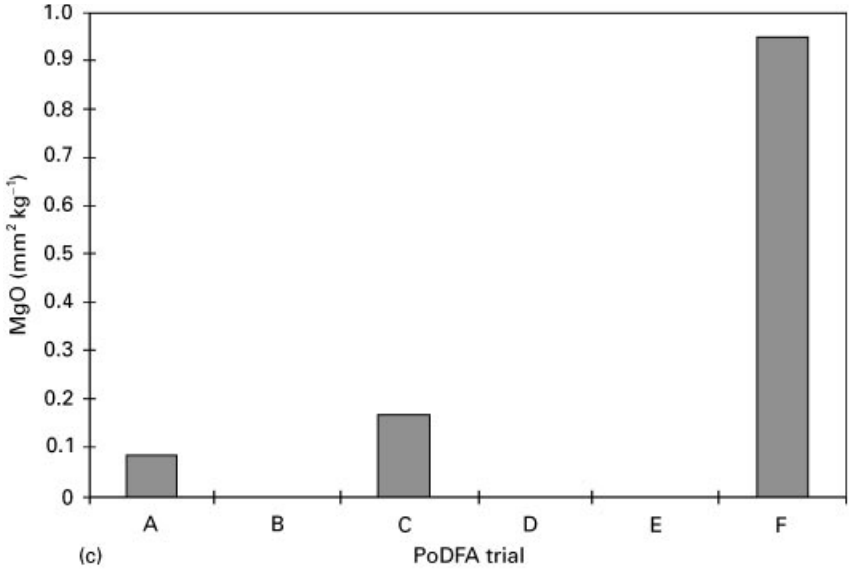

Figure 13 (Continued.)

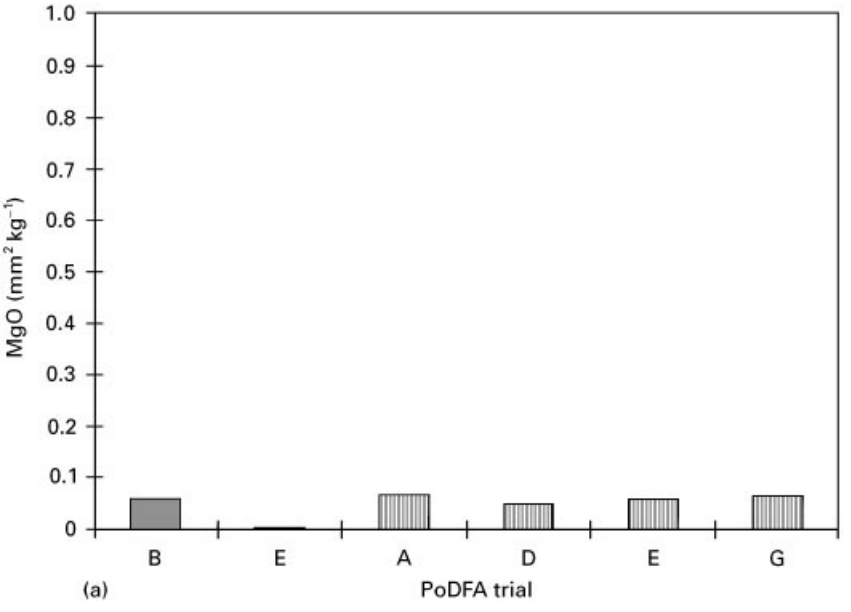

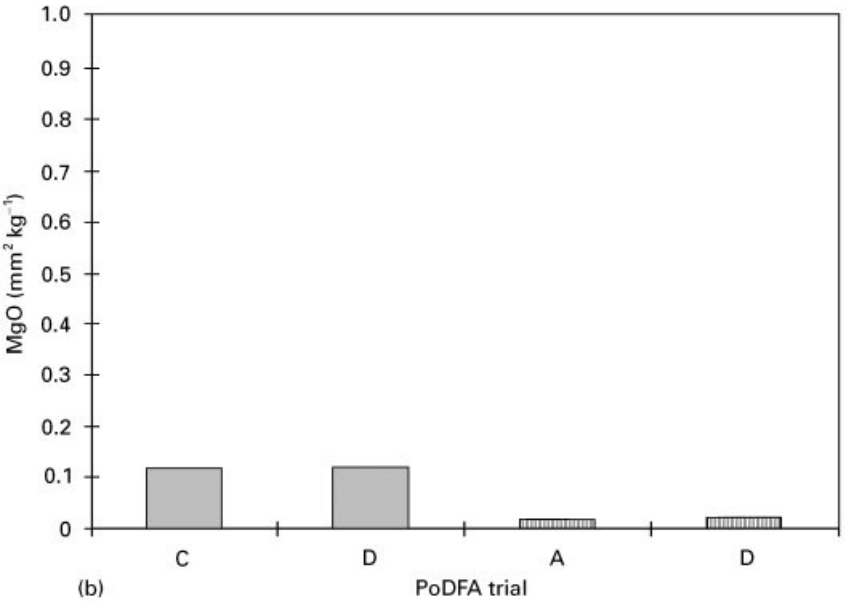

Figure 14 Experimental conditions that maximize the concentration of MgO inclusions in C357 alloy: (a) effect of settling time (( ), experiment 24; ( ), experiment 25); (b) effect of mechanical stirring (( ), experiment 27; ( ), experiment 28).

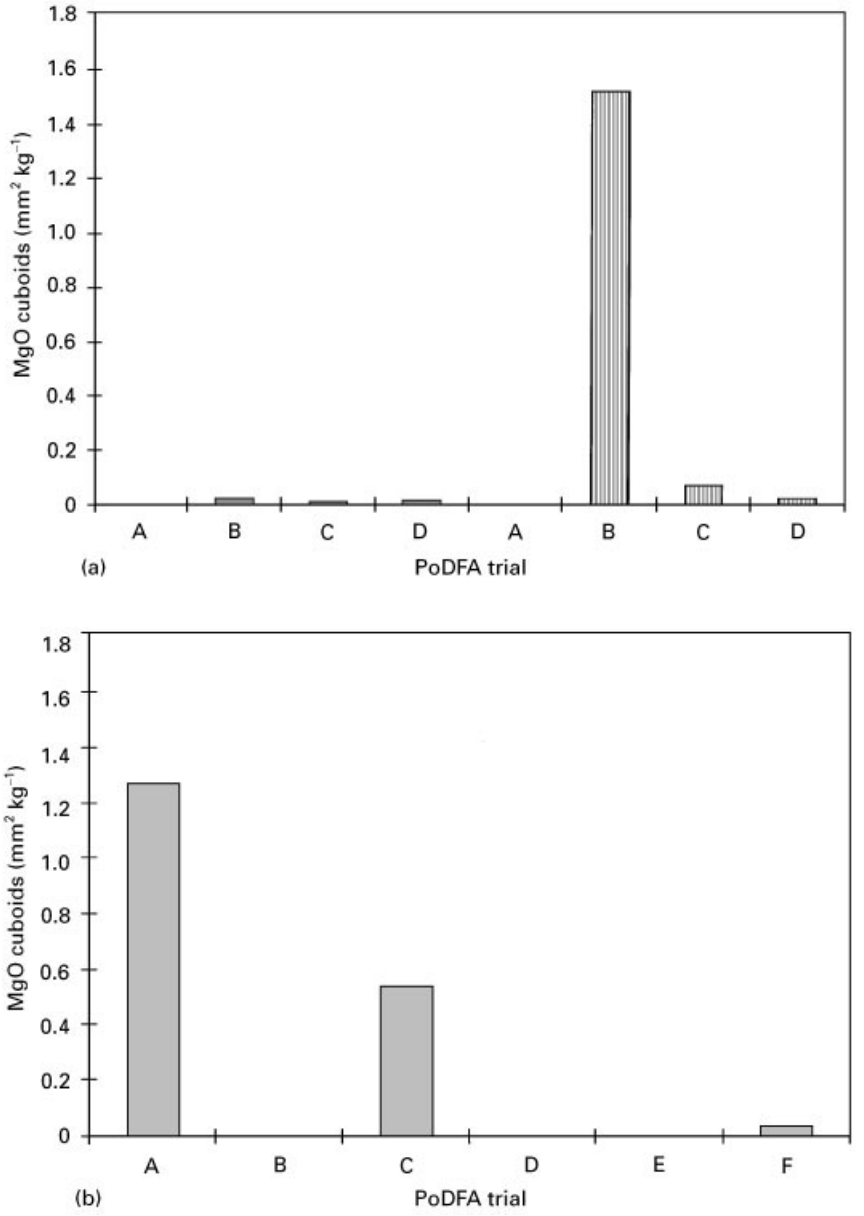

Figure 15 Experimental conditions that maximize the concentration of MgO cuboid inclusions in A356.2 alloy: (a) effect of the type of initial charge (( ), experiment 8; ( ), experiment 9); (b) effect of prolonged holding times, i.e., 72 h (( ), experiment 20).

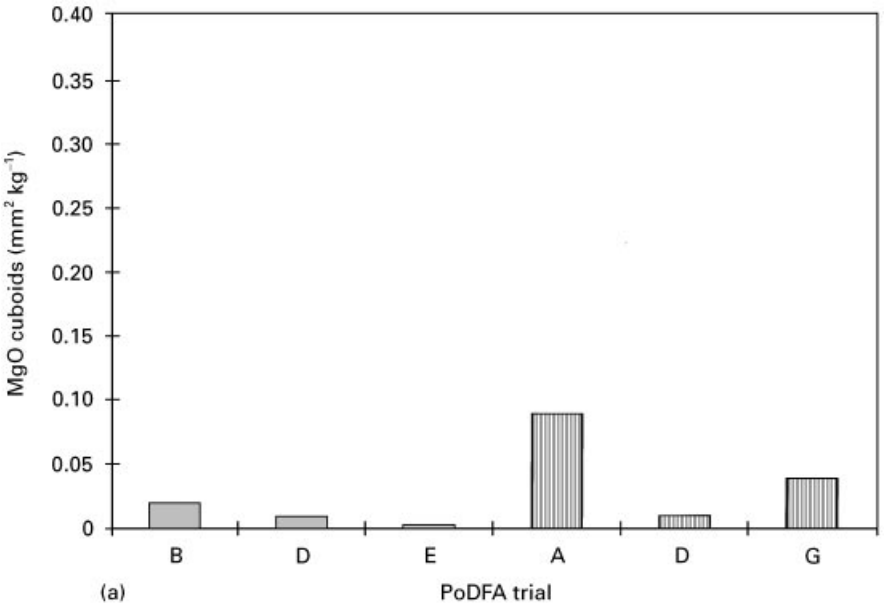

Figure 16 Experimental conditions that maximize the concentration of MgO cuboid inclusions in C357 alloy: (a) effect of settling time (( ), experiment 24; ( ), experiment 25); (b) effect of mechanical stirring (( ), experiment 27; ( ), experiment 28).

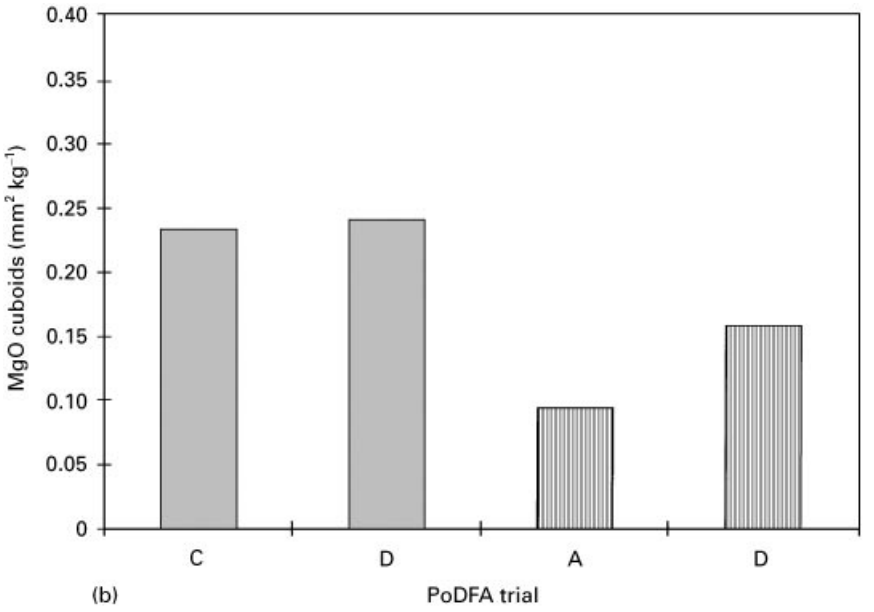

Figure 16 (Continued.)

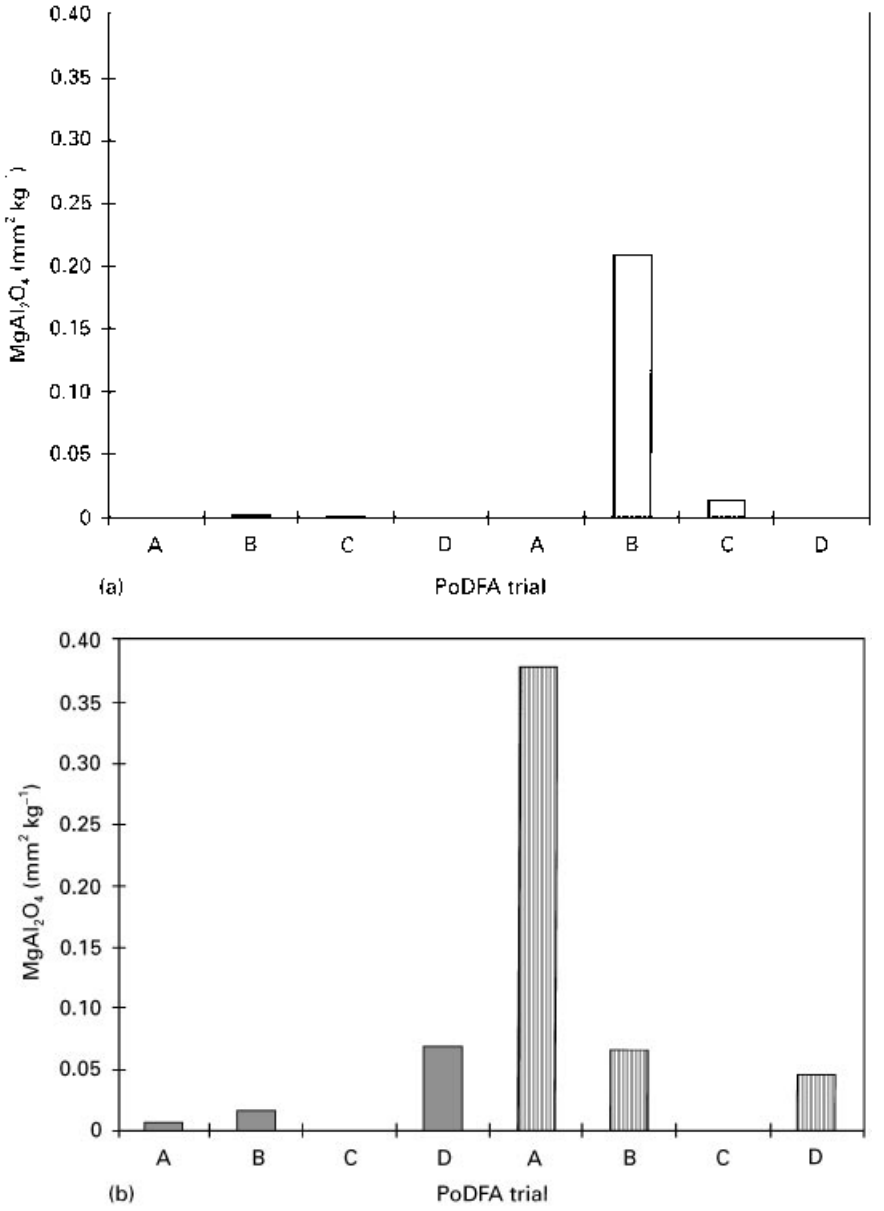

Figure 17 Experimental conditions that maximize the concentration of $MgAl_2O_4$ inclusions in A356.2 alloy: (a) effect of the type of initial charge ((▒), experiment 8; (▒), experiment 9); (b) effect of filtration conditions ((▒), experiment 16; (▒), experiment 17); (c) effect of prolonged holding times, i.e., 72 h ((▒), experiment 20).

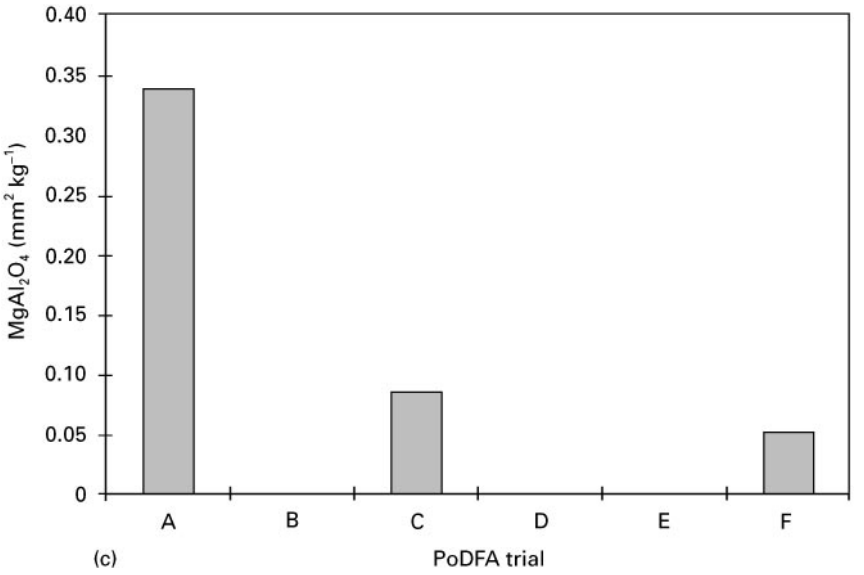

Figure 17 (Continued.)

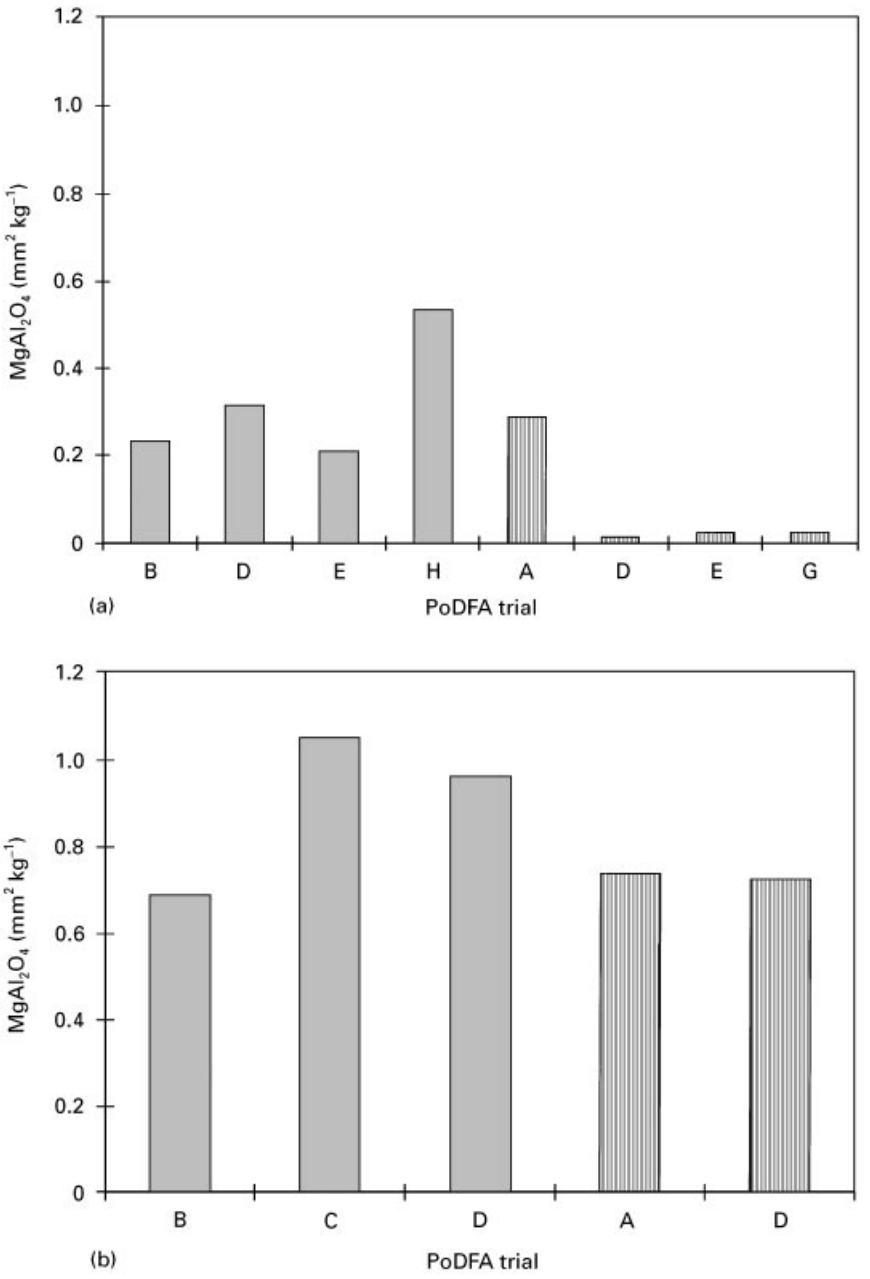

Figure 18 Experimental conditions that maximize the concentration of $MgAl_2O_4$ inclusions in C357 alloy: (a) effect of settling time (( ), experiment 24; ( ), experiment 25); (b) effect of mechanical stirring (( ), experiment 27; ( ), experiment 28).

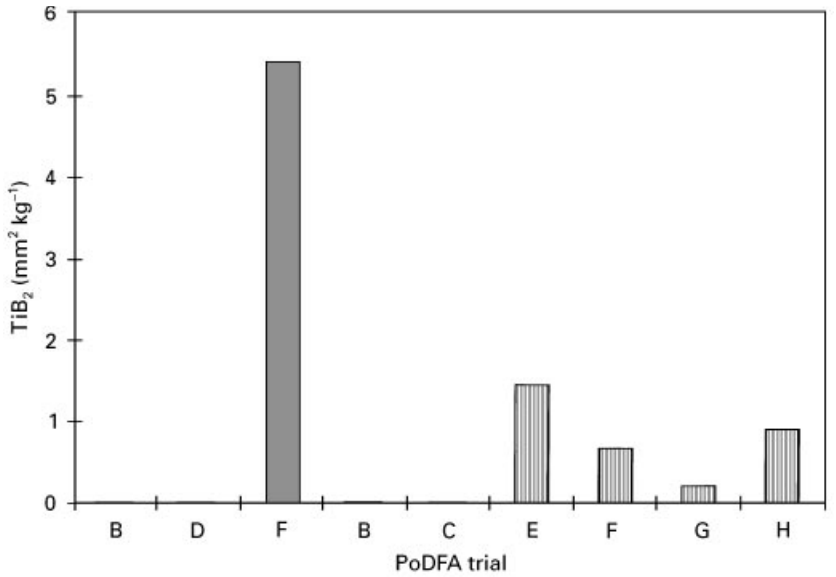

Figure 19 Experimental conditions that maximize the concentration of TiB_2 inclusions. ( ), experiment 21; ( ), experiment 22.

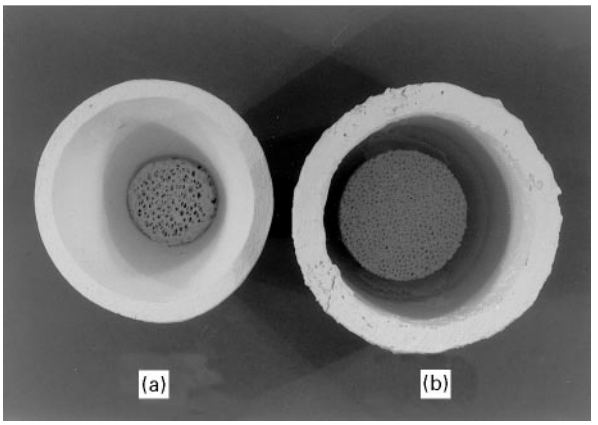

Figure 20 Pouring cups mounted with (a) 10 ppi and (b) 20 ppi ceramic foam filters.

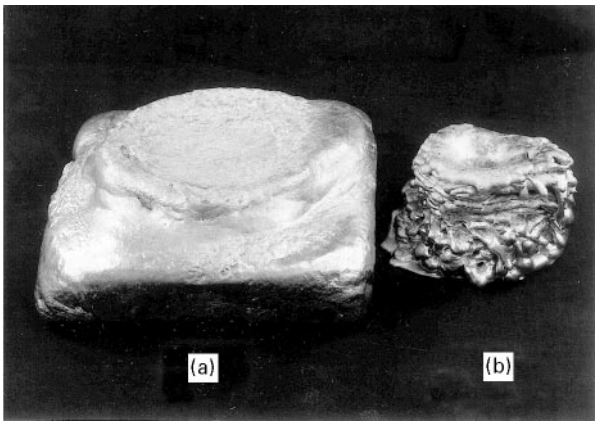

Figure 22 Effect of TiB_2 addition on the mass of filtered metal. (a) experiment 22A and (b) experiment 22E. Compare the droplet-like surface in experiment 22E with the smooth surface in experiment 22A.

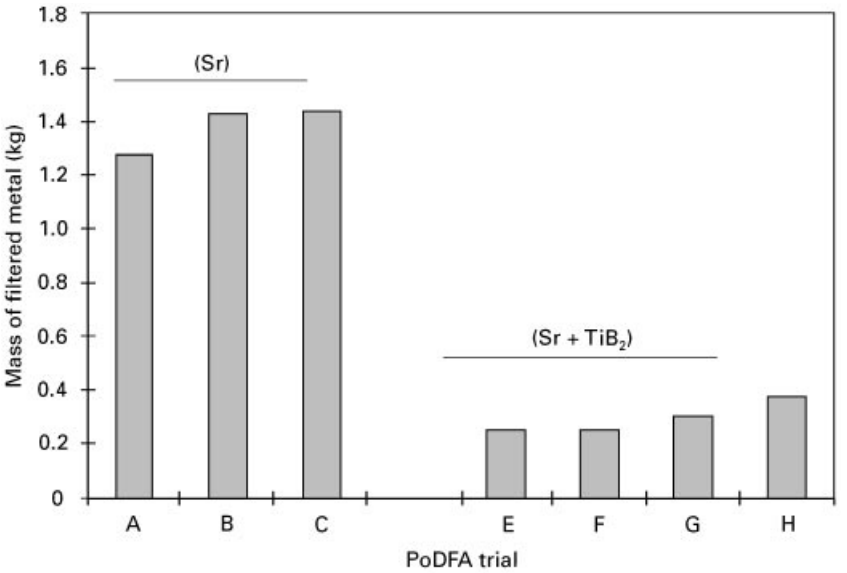

Figure 21 Effect of Sr and TiB_2 additions on the mass of filtered metal. ( ), experiment 22.

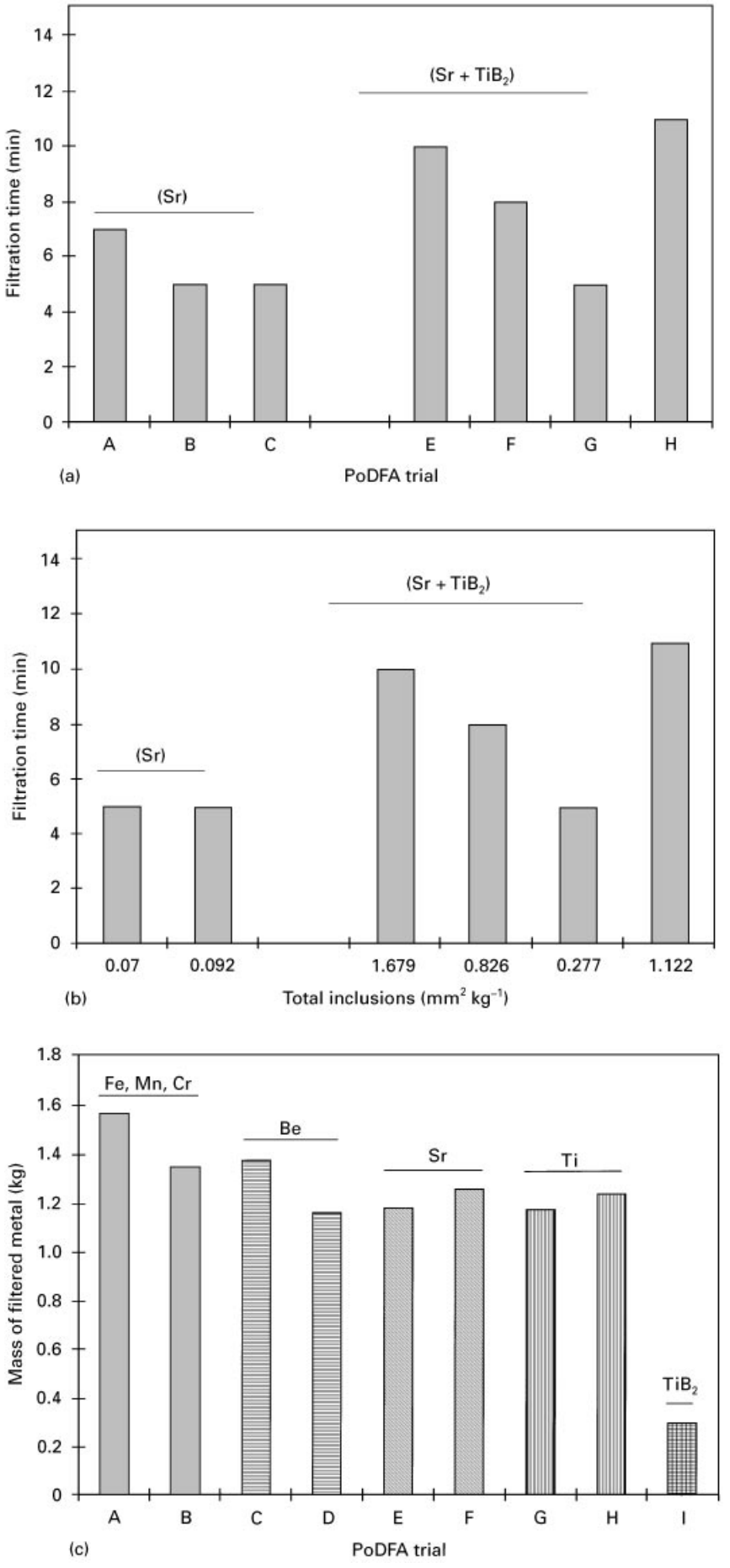

Figure 23 Effect of TiB_2 addition on (a) filtration time (( ), experiment 22), (b) total inclusions (( ), experiment 22) and (c) mass of filtered metal.

4. Conclusions

1. Mechanical stirring is one of the major parameters that contaminates the molten metal with inclusions. Degassing, on the other hand, using a rotary impeller, is very effective in removing the inclusions through flotation into the upper portion of the crucible. The thickness of the layer rich in inclusions, however, is determined by the degassing time and the amount of inert gas purged into the molten metal. It is, therefore, recommended that the first and last castings in a series of castings prepared from the same melt be rejected.

2. The use of ceramic foam filters in the pouring cup would greatly help to remove the oxide films provided that the pouring cup (containing the filter) is placed tightly at the top of the sprue without air gaps to avoid metal reoxidation.

3. Addition of alloying elements such as Sr, Fe, Mn, Cr and Be does not lead to inclusion formation if mechanical stirring is avoided. Another way of adding the alloying elements is by employing degassing.

4. A long holding time may lead to the sedimentation of several inclusions. However, in the case of Mg-containing alloys, i.e., A356 and A357, lengthy holding periods would accelerate the formation of high concentrations of cuboids and spinels near the surface.

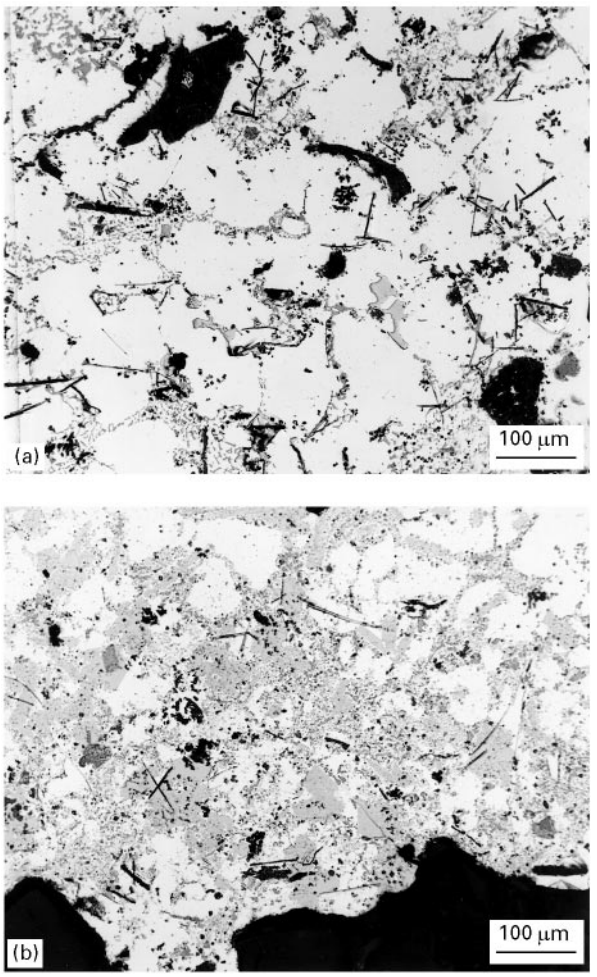

Figure 24 Effect of grain-refining agent type on the number of inclusion particles: (a) Al_3Ti; (b) TiB_2.

Acknowledgements

The financial and other support received from the Natural Sciences and Engineering Research Council of Canada, Centre Québécois de Recherche et de Développement de l'Aluminium (Chicoutimi, Québec, Canada), Alcan Smelters and Chemicals Ltd (Jonquière, Québec, Canada), Bomem, Inc. (Québec City, Québec, Canada), Cercast Group (Montreal, Québec, Canada), Grenville Castings Ltd (Merrickville, Ontario, Canada), General Motors Powertrain Group (Saginaw, MI, USA), KB Alloys, Inc. (Robards, KY, USA), Hi-Tech Ceramics, Inc. (New York, USA), Nemak–Alfa Industrial Group (Monterrey, Mexico) is gratefully acknowledged.

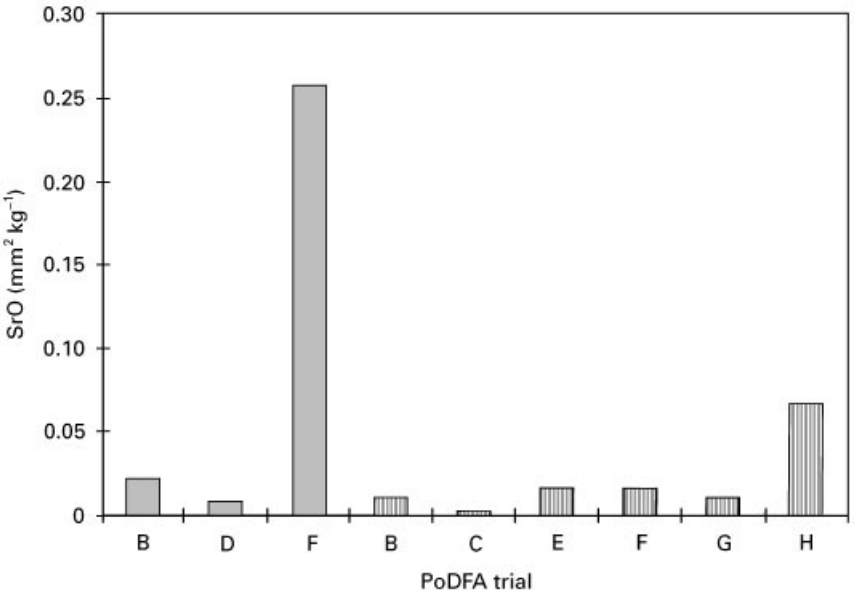

Figure 25 Experimental conditions that maximize the concentration of SrO inclusions in A356.2 alloy. ( ), experiment 21; ( ), experiment 22.

References

1. S. SHIVKUMAR, S. RICCI Jr, B. STEENHOFF, D. APELIAN and G. SIGWORTH, *Amer. Foundrymen's Soc. Trans.* **97** (1989) 791.
2. C. W. MEYERS and N. McRAY, in "Technology for Premium Quality Castings," edited by E. Dunn and D. R. Durham (Metallurgical Society of AIME, Warrendale, PA, 1988) p. 107.
3. D. APELIAN and S. SHIVKUMAR, *Amer. Foundrymen's Soc. Trans.* **97** (1989) 727.
4. K. J. OSWALT and M. S. MISRA, *ibid* **88** (1980) 845.
5. W. SIMMONS, *Indian Foundry J.*, (1988) 21.
6. C. J. SIMENSEN and G. BERG, *Aluminium* **56** (1980) 335.
7. D. APELIAN, in 1988 Electric Furnace Conference Proceedings, Pittsburgh 6–9 December, 1988, (Iron & Steel Society, Warrendale, PA, 1989) p. 325.
8. D. APELIAN, R. MUTHARASAN and S. ALI, *J. Mater. Sci.* **20** (1985) 350.
9. H. C. CUMMING, F. B. STULEN and W. C. SCHULTE, *Trans. Amer. Soc. Metals.* **49** (1957) 487.
10. C. E. ECKERT, R. E. MILLER, D. APELIAN and R. MUTHARASAN, *Light Metals* (1984) 1281.
11. C. J. SIMENSEN and H. VEDT, *Z. Metallkde* **76** (1985) 1179.
12. J. GORBRECHT, *Geisseri* **62** (1975) 263.
13. D. DOUTRE, B. GARIÈPY, J.-P. MARTIN and G. DUBÉ, *Light Metals* (1985) 1179.
14. S. JACOB, *Fonderie* **363** (1977) 13.
15. R. DASGUPTA, C. G. BROWN and S. MAREK, *Amer. Foundrymen's Soc. Trans.* **96** (1988) 297.
16. P. D. HESS and E. V. BLACKMUN, *ibid.* **84** (1975) 87.
17. D. APELIAN, G. V. SIGWORTH and V. R. WHALER, *ibid.* **92** (1984) 297.
18. L. F. MONDOLFO, "Grain Refinement in Castings and Welds", (Metallurgical Society of AIME, 1983) p. 3.
19. S. KENNERKNECHT, in "Advanced Casting Technology", AGARD/NATO Conference Proceedings No. 35. 54th meeting of the AGARD structures and Materials Panel in Brussels, Belgium, 4–9 April, 1982. (Advisory Group for Aerospace Research and Development, North Atlantic Treaty Organization AGARD/NATO, Brussels, 1982).
20. J. E. HATCH, (ed.) "Aluminium—Properties and Physical Metallurgy" (American Society for Metals, Metals Park, OH, 1984).
21. J. L. JORSTAD, *Die Casting Eng.* **30** (1986) 30.
22. A. M. SAMUEL and F. H. SAMUEL, *J. Mater. Sci.* **27** (1992) 6533.

Received 24 March
and accepted 1 May 1997